

# We are IntechOpen, the world's leading publisher of Open Access books Built by scientists, for scientists

6,900

Open access books available

185,000

International authors and editors

200M

Downloads

Our authors are among the

154

Countries delivered to

TOP 1%

most cited scientists

12.2%

Contributors from top 500 universities



WEB OF SCIENCE™

Selection of our books indexed in the Book Citation Index  
in Web of Science™ Core Collection (BKCI)

Interested in publishing with us?  
Contact [book.department@intechopen.com](mailto:book.department@intechopen.com)

Numbers displayed above are based on latest data collected.  
For more information visit [www.intechopen.com](http://www.intechopen.com)



---

# Terrestrial Coherent Free-Space Optical Communication Systems

---

Mingbo Niu, Julian Cheng and Jonathan F. Holzman

Additional information is available at the end of the chapter

<http://dx.doi.org/10.5772/48284>

---

## 1. Introduction

In the past three decades, the demand for high-speed communications has increased dramatically, while fiber optical communications has been applied in the majority of data transmission networks. Optical fiber has advantages over existing copper wire in long distance and high demand applications. The ever increasing need for higher bandwidth and higher speed optical data and communications transmission is driving the development of 100 gigabit per second (Gbit/s) communication links. However, infrastructure development within cities is relatively difficult and time-consuming, and fiber-optic systems are complex and expensive. Due to these difficulties, fiber-optic communication systems have primarily been installed in long-distance applications, where they can be used to their full transmission capacity, offsetting the increased cost.

The original free-space optical (FSO) communications white paper by Dr. Erhard Kube, "Information transmission by light beams through the atmosphere," was published in German in *Nachrichtentechnik*, June 1968. New advances in FSO technologies have led to a recent rebirth of optical broadband access as an attractive alternative for ultra high-speed networking. This can push forward the seamless development of the promising all-optical networks. In dense urban areas or places where optical fiber infrastructure does not exist, FSO communication systems have been shown to be a viable alternative [1]. Lower costs, larger license-free bandwidths, better information security, greater link flexibility, and a reduced time-to-market are all significant benefits of FSO communication systems [1]-[3]. FSO communications is a promising candidate to satisfy the new communication requirements due to its ability to transmit information at extremely high data rates using compact, low-mass terminals, while avoiding interference problems.

FSO communications, also known as the wireless optical communications, transmits optical signals through free-space. It requires line-of-sight (LOS) transmission, which means the transmitter and receiver at both networking locations must see each other. Whereas existing optical fiber is a predictable medium, FSO communications can suffer from cloud coverage

and harsh weather conditions leading to atmospheric effects which degrade the designed system availability and performance. Rain, snow, sleet, fog, etc. are limiting factors which can affect the transmission of laser beams through the atmospheric channels.

There are three primary atmospheric factors that can affect optical beam propagation: absorption, scattering, and refractive-index fluctuations (i.e., optical turbulence). Absorption and scattering are often grouped together under the topic of extinction, defined as the reduction or attenuation in the amount of radiation transmitting through the atmosphere. They are both deterministic effects that are fairly well-known and can be predicted by software packages such as FASCODE [4] or MODTRAN [5]. Nonetheless, optical turbulence is generally considered as the most serious optical effect on a propagating beam through atmospheric channels. In this chapter, we will focus on terrestrial coherent FSO systems in the presence of atmospheric turbulence.

### 1.1. Preliminaries on coherent free-space optical communications

Coherent fiber optical communications attracted considerable attention in the late 1980s for its ability to approach the theoretical receiver sensitivity limit. Similarly, FSO systems have great potential on improving channel usage when implemented with coherent detection [6]. One scheme of coherent FSO detection is called homodyne detection, where the receiver demodulates the optical signal directly to the baseband because the local oscillator laser frequency is synchronized to the optical signal carrier frequency. However, it can be unstable to perform optical synchronization in practice. As a result, heterodyne detection was introduced to simplify the receiver design and make coherent FSO systems more applicable. In heterodyne detection, the optical signal is first converted to an electrical signal with an intermediate frequency. Then a phase noise compensation scheme is used to track the phase noise of the IF signal. The received signals in coherent FSO systems can be made to be limited only by the shot noise of the incident optical power (given a sufficiently large local oscillator beam power). Furthermore, the extraction of phase information with these processes allows for a greater variety of modulation formats in comparison to irradiance-dependent detection schemes such as irradiance modulation with direct detection (IM/DD). The advantages of coherent FSO systems with phase noise compensation over IM/DD systems are excellent background noise rejection [7], higher sensitivity, and improved spectral efficiency (at the cost of higher system complexity). Note that the implementation and tradeoff of coherent FSO systems are beyond the scope of this chapter. More details can be found in [8]–[10]. Unlike coherent radio frequency (RF) communication links, coherent FSO systems utilize local oscillator and signal optical fields together with optical/electrical synchronization for the signal recovery.

An optical wave propagating through the atmosphere will experience irradiance fluctuations, also referred to as scintillation or turbulence-induced fading. Scintillation is caused by random fluctuations of refractive index due to temperature, pressure, and wind variations along the optical propagation path of the channel in the atmosphere. Theoretical and experimental studies generally center around the scintillation index, which is defined as the normalized variance of irradiance fluctuations

$$\sigma_{si}^2 = \frac{E[I^2] - (E[I])^2}{(E[I])^2} = \frac{E[I^2]}{(E[I])^2} - 1 \quad (1)$$

where the quantity  $I$  is the instantaneous optical irradiance and  $E[\cdot]$  denotes the expectation operation.

In weak turbulence regimes (when the scintillation index is less than unity), the scintillation index is found to be proportional to the Rytov variance [12], which is defined as

$$\sigma_R^2 = 1.23C_n^2 k^2 L_t^{\frac{11}{6}} \quad (2)$$

where  $C_n^2$  stands for the index of refraction structure parameter in  $m^{-2/3}$ ,  $k = 2\pi/\lambda_w$  is the optical wave number ( $\lambda_w$  denotes the wavelength), and  $L_t$  is the transmission path length between the transmitter and receiver. In (2),  $C_n^2$  is an altitude-dependent variable, and the most commonly used Hufnagle-Valley model for  $C_n^2$  is given by [12]

$$C_n^2 = 0.00594 \left( \frac{v}{27} \right)^2 (h \times 10^{-5})^{10} e^{\frac{h}{1000}} + 2.7e^{\frac{-h}{1500}} \times 10^{-6} + A_c e^{\frac{-h}{1000}} \quad (3)$$

where  $v$  is the root-mean-square wind speed in meters per second,  $h$  is the altitude in meters, and  $A_c$  is a nominal value of  $C_n^2$  at the ground. Typically, the value of  $C_n^2$  varies from approximately  $10^{-17}m^{-2/3}$  for weak turbulence conditions to  $10^{-13}m^{-2/3}$  for strong turbulence conditions (with  $10^{-15}m^{-2/3}$  as a typical average value) [13].

When the optical turbulence strength extends to moderate-to-strong irradiance fluctuation regimes (when the scintillation index is greater than unity) by increasing  $C_n^2$  and/or path length  $L_t$ , the scintillation index for a plane wave and that for a spherical wave are, respectively, related to the Rytov variance by [11]

$$(\sigma_{si}^2)_{plane} = \exp \left[ \frac{0.54\sigma_R^2}{(1 + 1.22\sigma_R^{\frac{12}{5}})^{\frac{7}{6}}} + \frac{0.509\sigma_R^2}{(1 + 0.69\sigma_R^{\frac{12}{5}})^{\frac{5}{6}}} \right] - 1 \quad (4)$$

and

$$(\sigma_{si}^2)_{sphere} = \exp \left[ \frac{0.17\sigma_R^2}{(1 + 0.167\sigma_R^{\frac{12}{5}})^{\frac{7}{6}}} + \frac{0.225\sigma_R^2}{(1 + 0.259\sigma_R^{\frac{12}{5}})^{\frac{5}{6}}} \right] - 1. \quad (5)$$

The performance of FSO communication systems can be significantly degraded by turbulence-induced scintillation. To be more specific, scintillation can lead to power loss at the photodetector and random fluctuations of the received signal below a predetermined detection threshold. The reliability of such FSO systems can be predicted by introducing mathematical models for the probability density function (PDF) of the instantaneous fading irradiance of the optical signal.

For the past several decades, the scientific community has investigated statistical models of turbulence-induced scintillation in FSO communications through the atmosphere. Of the turbulence-induced scintillation models introduced so far, the most commonly accepted models are the log-normal turbulence model (typically describing irradiance fluctuations in weak turbulence conditions),  $K$ -distributed turbulence model (typically describing irradiance fluctuations in strong turbulence conditions), and Gamma-Gamma turbulence model (providing a description of much wider irradiance fluctuation ranges across the weak to strong turbulence regimes). In the rest of this chapter, turbulence-induced scintillation is referred as (atmospheric) turbulence for simplicity unless stated otherwise.

This chapter is structured as follows. We first introduce the concept of coherent FSO communication and conduct a detailed literature review in the rest of Section 1. Section 2 will describe the system model of a coherent FSO link over atmospheric turbulence channels. We will analyze the signal-to-noise ratio (SNR) at the coherent FSO receiver and derive its expression in Section 2.1. A generalized atmospheric turbulence model and its characteristics will be presented in Section 2.2. In Section 3.1, we will present exact error rates for binary phase-shift keying (BPSK) using a moment generating function approach and a characteristic function approach. Furthermore, we will present asymptotic error rate analyses in Section 3.2 to offer further insights into system performance behavior in large SNR regimes. We will analyze outage probability in Section 3.3. Diversity techniques such as maximum ratio combining (MRC) and equal gain combining (EGC) will be employed to mitigate the turbulence effects in Section 4.1 and Section 4.2, respectively, and a performance comparison using numerical case studies will be presented in Section 4.3. We will also study the error rate performance degradation caused by phase noise compensation error in Section 5. When the standard deviation of the phase noise compensation error is large, we propose differential PSK (DPSK) as an effective alternative to BPSK in Section 5.3, as DPSK does not require the estimation of optical carrier phase. In Section 6, we summarize and conclude our important findings for coherent FSO systems and suggest further research topics on coherent FSO communications.

## 1.2. Literature review

FSO communications can be a key building block for future wide-area wireless data networks [14], [15] and can have great potential for applications in fourth-generation (4G) wireless systems [16]. Such systems are currently being deployed and will encompass a number of complementary access technologies with higher channel capacities, multiple antennas, and Gbit/s data rates [16]. Since the wireless optical transmission links are over the atmosphere, the laser beam propagating through turbulent channels is affected by scintillation and phase aberration, which can impair the system performance significantly.

In order to evaluate the system performance, an accurate model of turbulence is needed in error rate studies. In early studies of FSO communications, the log-normal distribution was used as the turbulence model [6], [17]–[22]. Although the log-normal distribution is one of the most widely used turbulence models, this PDF is only applicable for weak turbulence conditions. It was shown in [23]–[26] that the  $K$ -distributed turbulence model provides good agreement with experimental data in a variety of FSO experiments involving radiation scattered by strong turbulence. In a recent series of papers on scintillation theory [11], [27], Andrews *et al.* introduced the modified Rytov theory and the Gamma-Gamma PDF was proposed as a tractable mathematical model for a wide range of atmospheric turbulence levels. Other statistical models in the FSO literature to describe atmospheric turbulence are the log-normal Rician, Rayleigh and  $I - K$  models [28], [29], [44].

The performance of IM/DD FSO systems for different turbulence models has been well studied in the literature. Zhu and Kahn studied the employment of maximum likelihood sequence detection (MLSD) for IM/DD FSO links [21]. They further studied the pairwise error probability of coded FSO links assuming the turbulence to be log-normal distributed [22]. In [30], Uysal *et al.* studied the pairwise error probability of on-off keying (OOK) with temporally correlated  $K$ -distributed turbulence. Since FSO communications requires LOS

links, pointing errors can affect the FSO system performance if the detector aperture size is finite (non-negligible compared to the beam spot size). In [31], Farid and Hranilovic presented an FSO channel model which models the fading due to log-normal/Gamma-Gamma atmospheric turbulence and pointing errors by considering beam width, pointing error variance and detector size. A closed-form expression of fading PDF, including the combined effects of  $K$ -distributed turbulence and pointing errors as well as the bit-error rate (BER) expression for OOK were obtained by Sandalidis *et al.* in terms of the Meijer's  $G$ -function [32]. Sandalidis *et al.* further studied the BER performance of the same links but considered the misalignment (pointing errors) effects [32]. Later, Uysal extended their discussion of pairwise error probability for coded OOK FSO links to the cases with independent Gamma-Gamma turbulence [33]. Riediger *et al.* investigated a multiple symbol detection decision metric for OOK in both log-normal and Gamma-Gamma turbulence [34]. The results in these papers demonstrate that the performance of a single branch FSO link severely suffers from atmospheric turbulence and is far from satisfying the typical BER requirements for communication applications with practical SNRs. This necessitates the deployment of powerful fading-mitigation techniques.

In the existing literature on FSO communications, two techniques have been proposed to mitigate the degrading effects of atmospheric turbulence: error control coding in conjunction with interleaving [30], [33], and maximum likelihood sequence detection with the knowledge of joint temporal statistics of the turbulence [21]. However, both approaches come with some practical limitations. The first one requires large-size interleavers whereas the latter suffers from high computational complexity [20].

FSO systems using diversity reception can achieve significant performance improvements by mitigating the atmospheric channel turbulence. The use of spatial diversity was first proposed for FSO systems by Ibrahim and Ibrahim [43]. EGC and optimal combining have been shown to enhance the link outage performance with independent log-normal turbulence by Lee and Chan [17]. BERs of multiple-input multiple-output (MIMO) FSO systems with both independent and correlated log-normal turbulence was studied by Navidpour *et al.* [20]. In [21], a symbol-by-symbol maximum likelihood detector with spatial diversity in correlated log-normal turbulence was studied by Zhu and Kahn. In [37] and [38], Wilson *et al.* investigated MIMO FSO links employing pulse-position modulation (PPM) and  $Q$ -ary PPM with both Rayleigh and log-normal turbulence-induced fading. In a recent work, Tsiftsis *et al.* studied the  $K$  turbulence FSO link performance for an IM/DD system with OOK using optimal combining, EGC, and selection combining [40]. BER solutions that require multi-dimensional integrations were presented, and approximate BER expressions were also given using the Gaussian quadrature rule and an error function approximation based on the trapezoidal rule. Bayaki *et al.* studied MIMO IM/DD FSO links over the Gamma-Gamma turbulence and demonstrated a significant performance improvement by exploiting both transmitter and receiver diversity [41]. In a recent work, Abou-Rjeily and Slim studied the system performance for  $Q$ -ary PPM FSO systems with cooperative diversity (parallel multi-hop) over both Rayleigh and log-normal turbulence channels [42].

It is known that the best signal modulation format for IM/DD FSO systems is OOK, and the existing literature on IM/DD FSO mostly considers OOK modulation. However, to minimize the error rate, the OOK receiver requires the knowledge of the turbulence state in order to choose an optimum threshold. This implies the need for an adaptive decision threshold, which may be difficult to implement in a practical FSO system and is subject to channel

estimation errors. As a result, practical FSO systems typically adopt a fixed threshold to reduce the complexity. Such systems will utilize large transmit powers to overcome the impact of atmospheric turbulence. This leads to costly operation. In [48], Li *et al.* theoretically showed that a fixed threshold for IM/DD systems with OOK modulation will lead to suboptimal system performance. It is pointed out that the BER of OOK modulation is determined by both the turbulence level and the fixed threshold, and, therefore, can not be made arbitrarily small in the presence of atmospheric turbulence even when the SNR is asymptotically large. PPM modulation has been proposed as an error-floor-free alternative to the OOK modulation [37]–[39]. However, PPM modulation needs a complex transceiver design because of the tight synchronization requirements, and it also suffers from a poor bandwidth efficiency.

Coherent FSO communication is an attractive alternative to FSO communication systems using direct detection. It offers an improved frequency/spatial selectivity, higher spectral efficiency, better background noise rejection and increased detector sensitivity (compared to direct detection) while eliminating the need of the adaptive threshold in the IM/DD OOK systems. The main feature of coherent FSO systems is that the receiver of a coherent FSO system is limited only by local oscillator induced quantum noise when the power of the local oscillator (as will be discussed in Section 2.1) is sufficiently high. This is a significant difference from the intensity modulated FSO systems, for which background and thermal noise are the dominant factors affecting the error rate performance. Some comprehensive references to early work in this coherent FSO area can be found in [6] and [36]. Recently, a comparison study was carried out by Lee and Chan [18] and showed performance improvement of coherent detection over IM/DD detection in a log-normal environment. They compared the IM/DD and coherent FSO systems with their corresponding best modulation schemes and demonstrated theoretically that coherent FSO systems can lead to lower error rates. It was also found that coherent detection can provide additional outage probability improvement over direct detection [19].

With the benefits of coherent FSO in mind, exact BER expressions have been developed for DPSK over  $K$ -distributed turbulence [45]. As an extension to the work done in [45], Tsiftsis evaluated the BER performance of coherent FSO with DPSK in Gamma-Gamma distributed turbulence [46]. In both these works, however, a detailed system model and receiver SNR analysis for coherent FSO communication links were not presented. More recently, a heterodyne FSO system with pointing errors was studied by Sandalidis *et al.* for Gamma-Gamma turbulence channels [47]. In [47], closed-form fading statistics expressions that take into account both the turbulence and pointing error effects were derived in terms of the Meijer's  $G$ -function, and the BER expressions of DPSK for such cases were also developed. A statistical model was developed in [49] considering spatial phase noise with log-normal turbulence and analyzed for capacity evaluation [50], [51]. In [52] and [53], the error rate performance of coherent FSO systems with MRC, EGC, and selection diversity reception in strong turbulence regions was studied. Spatial diversity techniques have been shown to be effective in mitigating the atmospheric turbulence-induced fading. Recently, Belmonte and Kahn studied the performance of a coherent FSO link with a large effective aperture achieved by signal combining from multiple aperture arrays where a Gamma distribution is used to model irradiance fluctuations [54]. Aghajanzadeh and Uysal adopted the receiver model in [50] and studied the diversity-multiplexing tradeoff and the finite-SNR diversity gain for a single-input multiple-output coherent WOC system [55]. Later, they extended the work in [55] to a decode-and-forward multi-hop FSO relay link [56], which was shown to have an

impressive power saving over the multi-hop IM/DD system in log-normal turbulence via numerical studies. A recent experiment carried out by Lange *et al.* has demonstrated a 142 km terrestrial coherent FSO link using a homodyne BPSK scheme successfully with a data rate of 5.625 Gbit/s [57].

## 2. Coherent free-space optical system model

In this section, we present some background knowledge concerning wireless optical channels and the coherent FSO system model. We first address the fading characteristics of wireless propagation environments. We then introduce some basic concepts and the composition of a coherent FSO system, as shown in Fig. 1. Finally, we point out some technical challenges associated with coherent FSO communication systems.

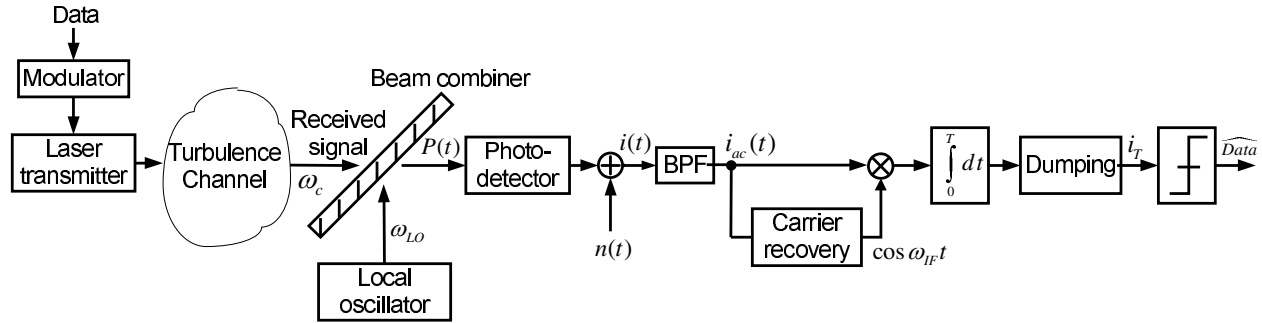


**Figure 1.** Block diagram of a typical coherent FSO system through an atmospheric turbulence channel.

### 2.1. Coherent free-space optical receiver

The main idea behind coherent optical systems lies in the mixing of the optical signal coherently with a continuous-wave local oscillator beam before it strikes the photodetector. By employing an optical local oscillator as well as a beamsplitter, we introduce a coherent FSO system for BPSK modulation in turbulence channels. The system model developed here gives a general idea on how coherent FSO systems are operated in turbulence channels.

In general optical communication systems, the current  $i_e(t)$  at the output of photodetector is comprised of multiple components [35], [58]

$$i_e(t) = i_p(t) + i_b + i_d + n_e(t) = \frac{\eta q}{h\nu} [P_{in}(t) + P_b] + i_d + n_e(t) \quad (6)$$

where the photocurrent  $i_p(t)$  represents the electrical photocurrent converted from the photodetector,  $i_b$  is the undesired background noise,  $i_d$  is the dark current (which is independent of the signal irradiance),  $n_e(t)$  is the total noise in a receiver circuit,  $P_{in}(t)$  is the received optical power,  $P_b$  is the background noise power and  $R = \eta q / (h\nu)$  is the responsivity defined in [59]. The total noise variance can be expressed as  $\sigma_{tot}^2 = \sigma^2 + \sigma_T^2$ , where  $\sigma^2$  and  $\sigma_T^2$  denote the variance of shot noise and thermal noise, respectively. Since  $\sigma^2$  and  $\sigma_T^2$  are independent of each other, we consider them separately. The variance  $\sigma^2$  of the shot noise is given by [59]

$$\sigma^2 = 2q[i_p(t) + i_b + i_d]\Delta f = 2q(RP_{in}(t) + i_b + i_d)\Delta f \quad (7)$$

where  $q$  is the electronic charge, and  $\Delta f$  is the noise equivalent bandwidth (NEB) of the photodetector. The thermal noise variance  $\sigma_T^2$  is given by

$$\sigma_T^2 = \frac{4kT\Delta f}{R_L} \quad (8)$$

where  $k$  is the Boltzmann constant,  $T$  is the absolute temperature in Kelvin, and  $R_L$  is the load resistance. In thermal noise dominant FSO systems, it can be readily seen that the total noise variance  $\sigma_{tot}^2 \doteq \sigma_T^2$  is independent of the incident optical power. In shot noise dominant FSO systems, the total noise variance  $\sigma_{tot}^2 \doteq \sigma^2$  is dependent on the incident optical power on the photodetector.

Since the ambient noise power is much stronger than the signal power in the free-space channel, shot noise due to ambient light and/or thermal noise is dominant in many IM/DD or subcarrier intensity modulated FSO systems. With the aid of a sufficiently large local oscillator power in a coherent FSO system, however, (local oscillator induced) shot noise can be made to be dominant, and the noise variance depends on the incident mixed optical irradiance. Thus, in a coherent FSO communication system, using the fact that the photocurrent from the receiver is the product of the responsivity  $R$  and incident optical power, we write the detected photocurrent from Fig. 1 as [53]

$$i(t) = i_{dc} + i_{ac}(t) + n(t) \quad (9)$$

where

$$i_{dc} = R(P_{in}(t) + P_{LO}) \doteq RP_{LO} \quad (10)$$

and

$$i_{ac}(t) = 2R\sqrt{P_{in}(t)P_{LO}} \cos(\omega_{IF}t + \phi_m) \quad (11)$$

represent the DC and AC terms at the receiver, respectively, and  $n(t)$  is a zero-mean AWGN process due to shot noise. In (11),  $\phi_m$  denotes the encoded phase information. In practice, an FSO system can be employed with  $P_{LO} \gg P_{in}(t)$ , and the DC term in (10) can be approximated by the dominant term  $RP_{LO}$ . For the same reason, photocurrent due to thermal noise and the dark current are negligible compared to  $RP_{LO}$ . The variance of the shot noise process  $n(t)$  is therefore found as [35]

$$\sigma_{n(t)}^2 = 2qRP_{LO}\Delta f. \quad (12)$$

The SNR of an optical receiver is ultimately defined as the ratio of the time-averaged AC photocurrent power to the total noise variance [59], and it can be expressed as

$$\gamma = \frac{\langle i_{ac}^2(t) \rangle}{\sigma_{tot}^2} \quad (13)$$

where  $\langle \cdot \rangle$  denotes the time average.

For coherent synchronous detection with  $M$ -ary constant amplitude modulation, we have  $P_{in}(t) = P_s$  and obtain that the instantaneous SNR as

$$\gamma = \frac{4R^2P_sP_{LO}}{2\sigma_{n(t)}^2} = \frac{RP_s}{q\Delta f}. \quad (14)$$

Let us define  $E_s$  to be the symbol energy of the  $M$ -ary constellation. Using the relationship that the optical power is the product of optical signal irradiance and photodetector area  $A$ , we can also write the SNR per symbol as

$$\gamma = \frac{RE_s A}{q\Delta f} I = \frac{\eta_e E_s A}{h\nu\Delta f} I = E_s C I \quad (15)$$

where  $\eta_e$  denotes the quantum efficiency of the photodetector,  $h$  is Planck's constant,  $\nu$  denotes the frequency of the received optical signal, and  $C = \eta_e A / (h\nu\Delta f)$  is a multiplicative constant for a given FSO system. Note that the instantaneous SNR is independent of the local oscillator power  $P_{LO}$ .

## 2.2. Terrestrial free-space optical channels

The random variation in signal irradiance resulting from atmospheric turbulence is a major source of system performance degradation in FSO communication systems. To address and mitigate such link performance degradation caused by turbulence channels, researchers have studied wireless optical channels extensively and proposed different channel models [14]-[22]. The turbulence effects, which are mainly due to the fluctuation of the refractive index, can be categorized by the range of scintillation index indicating the strength of turbulence-induced fading. In this section, we will briefly describe log-normal,  $K$ , Gamma-Gamma and negative exponential turbulence models.

### 2.2.1. Log-normal turbulence

When the optical channel is considered as a clear-sky atmospheric turbulence channel with several hundred meters propagation distance, the optical turbulence can be modeled as log-normal distribution. The corresponding weak turbulence range of scintillation index for log-normal is less than unity. Thus, although a log-normal model can be valid for longer propagation distances, the condition  $\sigma_{si}^2 < 1$  limits the log-normal model with longer propagation distances to be only used for a small index of refraction structure constant  $C_n^2$  [45]. This can be clearly observed from (2), which describes the relationship between scintillation index (i.e., Rytov variance) and propagation distance under weak turbulence conditions.

For weak turbulence conditions, Parry [24], Phillips and Andrews [25] independently suggested a log-normal PDF to model the irradiance, which is the power density of the optical beam. With a log-scale parameter  $\lambda$ , the log-normal PDF of the irradiance  $I$  can be expressed as [12]

$$f_{LN}(I) = \frac{1}{I\sqrt{2\pi\sigma_{si}^2}} \exp\left\{-\frac{[\ln I - \lambda]^2}{2\sigma_{si}^2}\right\}, \quad I > 0. \quad (16)$$

If we let  $\lambda = -\frac{1}{2}\sigma_{si}^2$ , the mean irradiance can be normalized to be  $E[I] = \exp(\lambda + \sigma_{si}^2/2) = e^0 = 1$ . The  $n$ th moment of the log-normal PDF is

$$E[I^n] = \exp[n\lambda + n^2\sigma_{si}^2/2]. \quad (17)$$

When turbulence levels increase further, the negative exponential distribution can be applied as a limiting distribution for the irradiance fluctuation. This limiting distribution can only provide sufficient accuracy when the system goes into the deep saturation regime [28].

### 2.2.2. *K*-distributed turbulence

One of the widely accepted models under the strong turbulence regime is the *K*-distributed turbulence model. In the 1970s, Jakeman *et al.* introduced this turbulence model for a non-Rayleigh sea echo. They have shown that the *K* distribution arises from the limiting form when the average number of multi-path fluctuations becomes large in the random sinusoid model [60]. Then Phillips and Andrews proved the validity of this *K* distribution by experiments in the strong turbulence regime [24], [25]. The *K*-distribution is an accurate model of turbulence if moderate propagation distances are encountered (about 1km) or the scintillation index [11] is confined to the range (2, 3) [45].

The *K*-distributed FSO turbulence is modeled as follows [45]:

$$f_K(I) = \frac{2}{\Gamma(\alpha)\eta^{\alpha+1}} \alpha^{\frac{\alpha+1}{2}} I^{\frac{\alpha-1}{2}} K_{\alpha-1} \left( \frac{2}{\eta} \sqrt{\alpha I} \right), \quad I \geq 0 \quad (18)$$

where  $\Gamma(\cdot)$  denotes the gamma function,  $K_x(\cdot)$  is the modified Bessel function of the second kind of order  $x$ ,  $\eta^2$  is the mean irradiance of the optical signal,  $\alpha$  is a channel parameter related to the effective number of discrete time scatterers and/or scintillation index. The  $n$ th moment of the *K* distribution can be shown to be

$$E[I^n] = \frac{\Gamma(\alpha + n)\eta^{2n}n!}{\alpha^n\Gamma(\alpha)}. \quad (19)$$

### 2.2.3. Gamma-gamma turbulence

In [11], Andrews *et al.* proposed the modified Rytov theory which defines the optical field as a function of perturbations due to large-scale and small-scale atmospheric effects. This leads to the Gamma-Gamma turbulence model. The PDF of the Gamma-Gamma distribution is

$$f_G(I) = \frac{2(\alpha\beta)^{(\alpha+\beta)/2}}{\Gamma(\alpha)\Gamma(\beta)I_0} \left( \frac{I}{I_0} \right)^{\frac{\alpha+\beta}{2}-1} K_{\alpha-\beta} \left( 2\sqrt{\alpha\beta\frac{I}{I_0}} \right), \quad \alpha > 0, \beta > 0, I \geq 0 \quad (20)$$

where  $I_0$  denotes the mean irradiance,  $\alpha$  and  $\beta$  represent, respectively, the effective number of large-scale and small-scale cells of the scattering process. Note that by setting the shape parameter  $\beta = 1$ , the Gamma-Gamma distribution will degenerate to the *K*-distribution. The Gamma-Gamma turbulence model is desirable for both weak and strong turbulence scenarios, because this model can provide a good fit to such experimental measurements of irradiance [27]. Therefore, the key advantage of using the Gamma-Gamma turbulence model is that it covers a wide-range of turbulence conditions.

The  $n$ th moment of the Gamma-Gamma PDF is found as

$$E[I^n] = \frac{\Gamma(\alpha + n)\Gamma(\beta + n)}{\Gamma(\alpha)\Gamma(\beta)} \left( \frac{I_0}{\alpha\beta} \right)^n. \quad (21)$$

It can be shown that the channel parameters  $\alpha$  and  $\beta$  are determined through the Rytov variance  $\sigma_R^2$  defined in (2) [12], so that they are not arbitrarily chosen. The relationship  $\alpha > \beta$  holds in most FSO scenarios, as shown in Fig. 2 and Fig. 3, though the reverse relationship

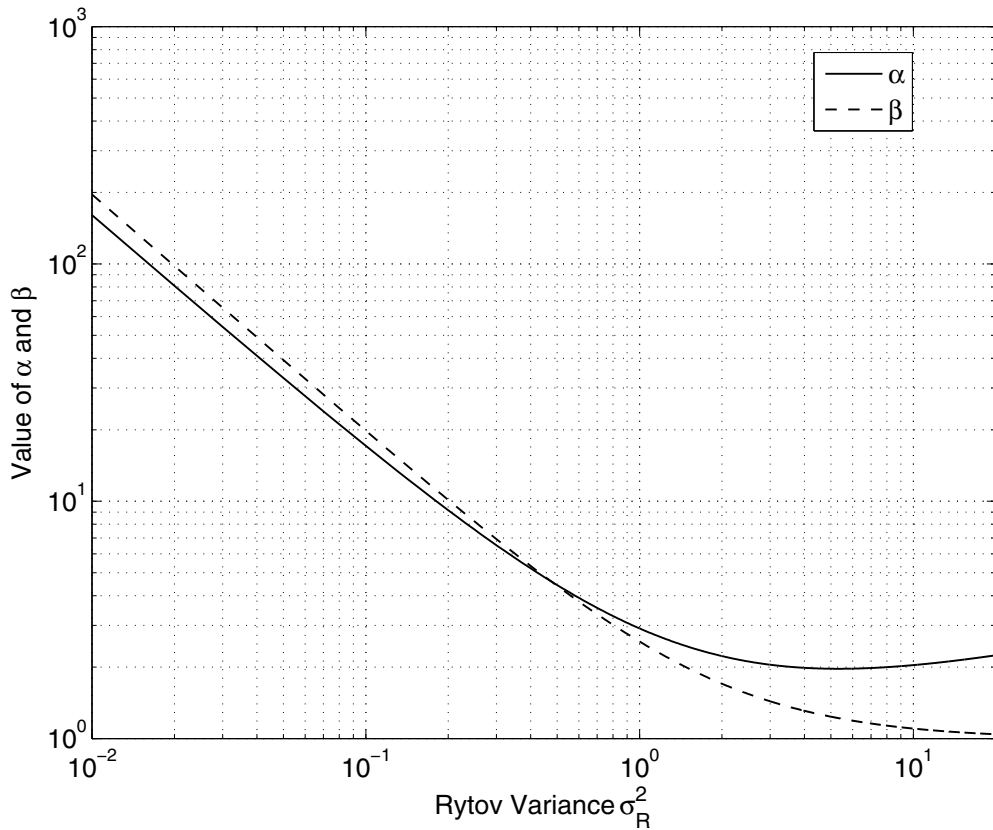


**Figure 2.** The relationship of the Gamma-Gamma turbulence channel parameters  $\alpha$  and  $\beta$  with the Rytov variance  $\sigma_R^2$  for a finite inner scale  $l_0 = R_F/2$  where  $R_F$  is the radius of the first fresnel zone.

$\beta > \alpha$  may appear in weak turbulence regimes when the inner-scale  $l_0$  is non-negligible. When considering spherical wave propagation,  $\alpha$  and  $\beta$  can be directly linked to the physical parameters through [12]

$$\alpha = \left\{ \exp \left[ \frac{0.49\chi^2}{(1 + 0.18d^2 + 0.56\chi^{12/5})^{7/6}} \right] - 1 \right\}^{-1} \quad (22)$$

and

$$\beta = \left\{ \exp \left[ \frac{0.51\chi^2(1 + 0.69\chi^{12/5})^{-5/6}}{(1 + 0.9d^2 + 0.62d^2\chi^{12/5})^{5/6}} \right] - 1 \right\}^{-1} \quad (23)$$

where  $\chi^2 = 0.5C_n^2 k^{7/6} L_t^{11/6}$  and  $d = (kD_a^2/4L_t)^{1/2}$ , and where  $D_a$  denotes the diameter of the receiver collecting lens aperture.

#### 2.2.4. Negative exponential turbulence

The negative exponential distribution is considered to be a limiting turbulence model case for describing irradiance fluctuations in the deep saturation regime. In negative exponential turbulence environments, the irradiance is modeled as a negative exponential RV having a PDF [44]

$$f_{\text{NE}}(I) = \lambda \exp(-\lambda I), \quad I \geq 0 \quad (24)$$

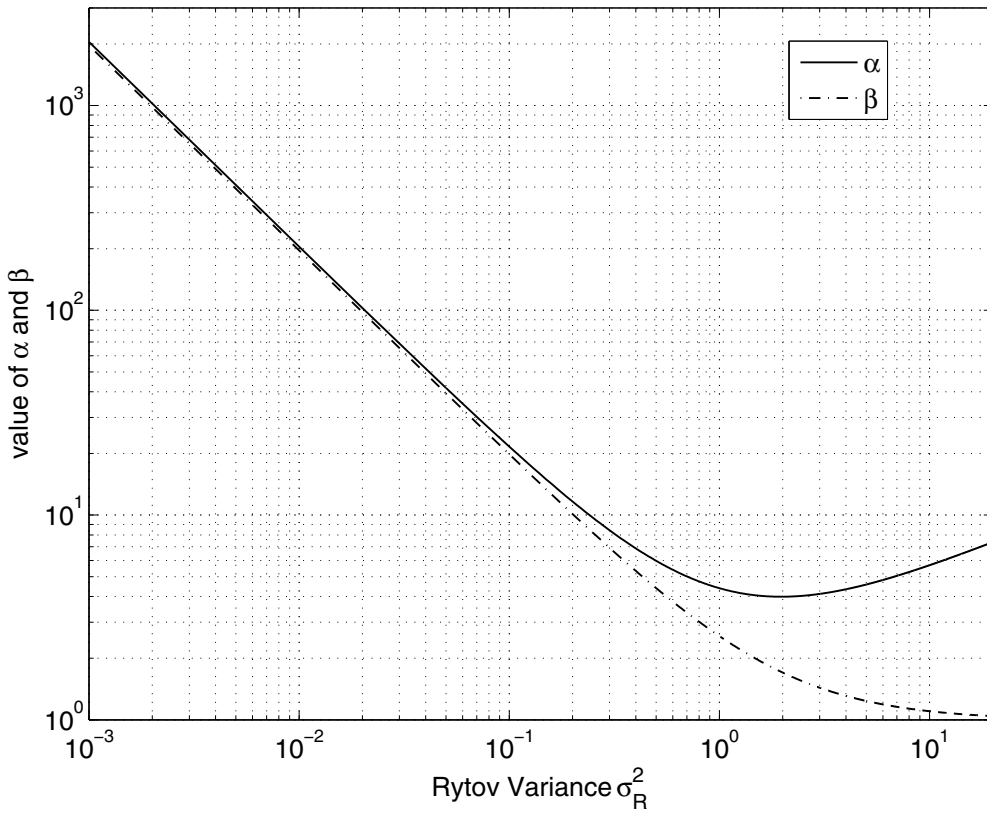


**Figure 3.** The relationship of Gamma-Gamma turbulence channel parameters  $\alpha$  and  $\beta$  as a function of the Rytov variance  $\sigma_R^2$  with negligible inner scale, i.e.,  $l_0 \rightarrow 0$ .

where  $1/\lambda > 0$  is the mean irradiance. The  $n$ th moment of the negative exponential distribution is

$$E[I^n] = \frac{n!}{\lambda^n}. \quad (25)$$

The negative exponential model can be considered to be a special case of the  $K$ -distributed model. The  $K$ -distribution approaches the negative exponential distribution when the channel parameter  $\alpha$  approaches  $\infty$ , i.e., irradiance fluctuations approach the deep saturation regime.

### 3. System performance analysis over a single free-space optical link

In this section, we present error rate results on coherent FSO communications in general Gamma-Gamma turbulence channels (weak-to-strong regimes). The average error rate of FSO systems over a turbulence channel can be expressed as

$$P_e = \int_0^\infty P_e(I) f(I) dI \quad (26)$$

where  $P_e(I)$  denotes the conditional symbol error probability and  $f(I)$  is the PDF of the received optical irradiance. To facilitate the system analyses, we study the statistics of the Gamma-Gamma distribution related to the instantaneous SNR.

The moment generating function (MGF) of irradiance  $I$  is defined as

$$M_I(s) = \int_0^\infty e^{sI} f(I) dI = E[e^{sI}]. \quad (27)$$

With [63, Eq. 6.643(3), Eq. 9.220(2), Eq. 9.220(3), Eq. 9.220(4)], we obtain the MGF of  $I$  as

$$M_I(s) = \frac{(\alpha\beta)^{\frac{\alpha+\beta}{2}} \exp\left(-\frac{\alpha\beta}{s}\right)}{\sqrt{\alpha\beta}} (-s)^{-\frac{\alpha+\beta-1}{2}} \left[ \frac{\Gamma(\beta-\alpha)}{\Gamma(\beta)} \left(-\frac{\alpha\beta}{s}\right)^{\frac{\alpha-\beta+1}{2}} {}_1F_1\left(\alpha, \alpha-\beta+1; -\frac{\alpha\beta}{s}\right) + \frac{\Gamma(\alpha-\beta)}{\Gamma(\alpha)} \left(-\frac{\alpha\beta}{s}\right)^{\frac{\beta-\alpha+1}{2}} {}_1F_1\left(\beta, \beta-\alpha+1; -\frac{\alpha\beta}{s}\right) \right] \quad (28)$$

where  ${}_1F_1(\cdot, \cdot; \cdot)$  denotes the confluent hypergeometric function. We comment that by replacing  $s$  with  $j\omega$  in (28) one can readily obtain the characteristic function (CHF) of the irradiance  $I$ .

### 3.1. Error rate analysis

Using the alternative form of the Gaussian  $Q$ -function,

$$Q(x) = \frac{1}{\pi} \int_0^{\frac{\pi}{2}} \exp\left(-\frac{x^2}{2\sin^2\theta}\right) d\theta, \quad x > 0 \quad (29)$$

we can express the average symbol-error rate (SER) of  $M$ -ary phase-shift keying (MPSK) as [61]

$$P_{e, MPSK} = \frac{1}{\pi} \int_0^{\frac{(M-1)\pi}{M}} M_I\left(-\frac{\sin(\pi/M)^2 \bar{\gamma}}{2\sin^2\theta}\right) d\theta \quad (30)$$

where  $\bar{\gamma} = CE_s$  is the average SNR. When  $M = 2$ , we can express the average BER with BPSK as

$$P_{e, BPSK} = \frac{1}{\pi} \int_0^{\frac{\pi}{2}} M_I\left(-\frac{\bar{\gamma}}{2\sin^2\theta}\right) d\theta. \quad (31)$$

Closed-form SER and BER expressions can then be obtained from (30) and (31) via a series expansion approach. Substituting (20) and a series expansion of the modified Bessel function of the second kind [41, Eq. (6)], [62, Eq. (03.04.06.0002.01)],

$$K_\nu(x) = \frac{\pi}{2\sin(\pi\nu)} \sum_{p=0}^{\infty} \left( \frac{(x/2)^{2p-\nu}}{\Gamma(p-\nu+1)p!} - \frac{(x/2)^{2p+\nu}}{\Gamma(p+\nu+1)p!} \right), \quad \nu \notin \mathbf{Z}, \quad |x| < \infty \quad (32)$$

into (26) and using integral identities [63, Eq. 3.621(1), Eq. 8.384(4)], we can express the SER for MPSK modulated coherent FSO systems as

$$P_{e, MPSK} = \frac{B(\alpha-\beta, 1-\alpha+\beta)}{\pi} \sum_{p=0}^{\infty} \left[ \frac{a_p(\alpha, \beta) \Gamma(p+\beta) \varphi(p+\beta, M)}{\sin^{2p+2\beta}\left(\frac{\pi}{M}\right)} \left(\frac{\bar{\gamma}}{2}\right)^{-(p+\beta)} - \frac{a_p(\beta, \alpha) \Gamma(p+\alpha) \varphi(p+\alpha, M)}{\sin^{2p+2\alpha}\left(\frac{\pi}{M}\right)} \left(\frac{\bar{\gamma}}{2}\right)^{-(p+\alpha)} \right] \quad (33)$$

where we define

$$a_p(\alpha, \beta) \triangleq \frac{(\alpha\beta)^{p+\beta}\Gamma(\alpha-\beta)\Gamma(\beta-\alpha+1)}{\Gamma(\alpha)\Gamma(\beta)\Gamma(p-\alpha+\beta+1)p!}. \quad (34)$$

Here,  $\varphi(x, M)$  denotes an integral identity from Mathematica<sup>®</sup> defined as

$$\begin{aligned} \varphi(x, M) &= \int_0^{\frac{M-1}{M}\pi} \sin^{2x} \theta d\theta \\ &= \frac{\pi^{\frac{3}{2}} \sec(\pi x)}{2\Gamma(x+1)\Gamma(\frac{1}{2}-x)} {}_2F_1\left(\frac{1}{2}, \frac{1}{2} - x; \frac{3}{2}; \cos^2 \frac{(M-1)\pi}{M}\right) \end{aligned} \quad (35)$$

where  ${}_2F_1(\cdot, \cdot; \cdot; \cdot)$  denotes the Gaussian hypergeometric function [63, Eq. 9.100]. Again, substituting (32) into (26) and using [63, Eq. 3.478(1), Eq. 3.621(1), Eq. 8.384(1), Eq. 8.384(4)], one can similarly obtain the closed-form average BER for BPSK coherent FSO systems as

$$\begin{aligned} P_{e, BPSK} &= \frac{B(\alpha-\beta, 1-\alpha+\beta)}{2\pi} \sum_{p=0}^{\infty} \left[ a_p(\alpha, \beta)\Gamma(p+\beta)B\left(\frac{1}{2}, p+\beta+\frac{1}{2}\right) \left(\frac{\bar{\gamma}}{2}\right)^{-(p+\beta)} \right. \\ &\quad \left. - a_p(\beta, \alpha)\Gamma(p+\alpha)B\left(\frac{1}{2}, p+\alpha+\frac{1}{2}\right) \left(\frac{\bar{\gamma}}{2}\right)^{-(p+\alpha)} \right] \end{aligned} \quad (36)$$

where  $B(x, y) = \Gamma(x)\Gamma(y)/\Gamma(x+y)$  denotes the Beta function [63, Eq. 8.384(1)] which is defined as

$$B(x, y) \triangleq \int_0^1 t^{x-1}(1-t)^{y-1} dt, \quad \Re\{x\} > 0, \Re\{y\} > 0. \quad (37)$$

Note that the condition  $(\alpha - \beta) \notin \mathbf{Z}$  holds for most values of  $\sigma_R^2$ , i.e., most terrestrial FSO scenarios, as shown in Fig. 2 and Fig. 3. If needed, we can change the difference between  $\alpha$  and  $\beta$  via varying  $\sigma_R^2$  by a small constant  $\epsilon$  to approximate the scenario when  $(\alpha - \beta) \in \mathbf{Z}$  (corresponding to a specific  $\sigma_R^2$  value).

The error rates of coherent MPSK systems are shown for both weak ( $\alpha = 3.0, \beta = 2.7$ ) and strong ( $\alpha = 2.3, \beta = 1.1$ ) turbulence channels in Fig. 4. As the modulation index  $M$  increases, it is clearly seen that the error rate degrades due to the symbol power constraints.

### 3.2. Asymptotic performance analysis

The asymptotic approach is a powerful method since the asymptotic solutions can often be used to reveal important insights of the target system behavior in large SNR regimes. For the Gamma-Gamma turbulence model, we have  $\alpha > \beta$  in most scenarios. Therefore, without losing of generality, we assume  $\alpha > \beta$  in asymptotic studies. We observe from (33) and (36) that the term  $(0.5\bar{\gamma})^{-\alpha}$  decreases faster than the term  $(0.5\bar{\gamma})^{-\beta}$  as  $\bar{\gamma}$  increases for given  $p$  values. Consequently, when  $\bar{\gamma}$  increases, the SER of MPSK modulation in large SNR regimes for coherent FSO systems over the Gamma-Gamma channel can be approximated by

$$P_{e, asym}^{\text{MPSK}} = \frac{a_0(\alpha, \beta)B(\alpha-\beta, 1-\alpha+\beta)\Gamma(\beta)\varphi(\beta, M)}{\pi \sin^{2\beta}(\frac{\pi}{M})} \left(\frac{\bar{\gamma}}{2}\right)^{-\beta}. \quad (38)$$

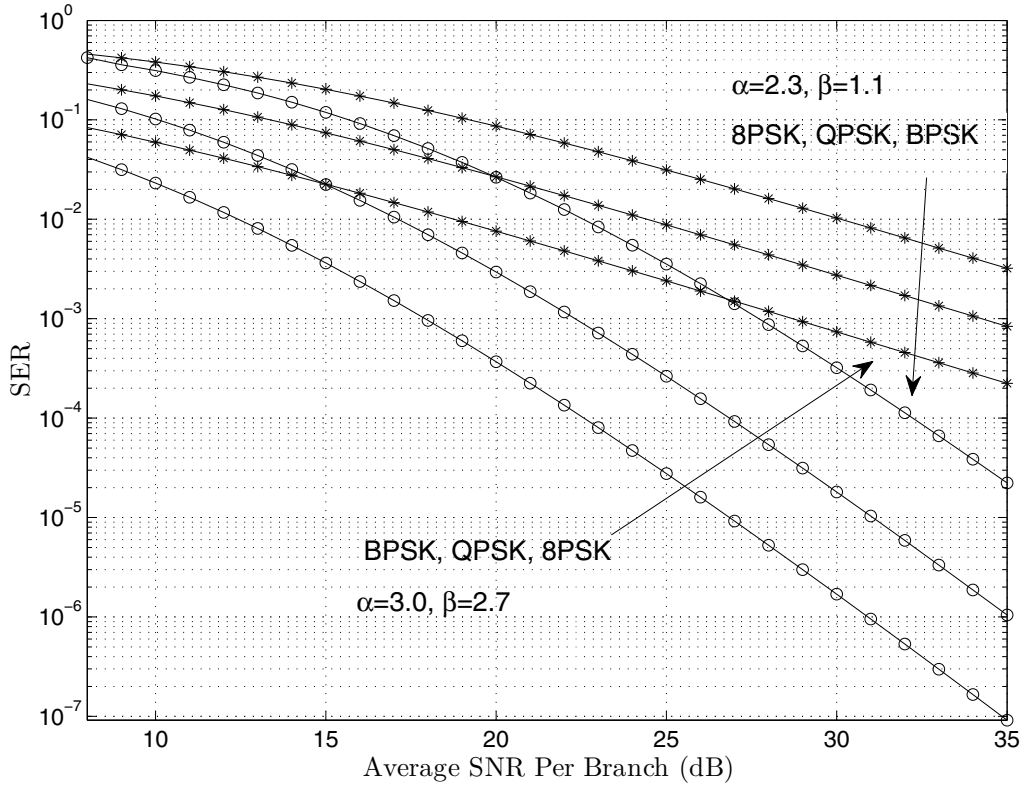


**Figure 4.** SER comparison of coherent MPSK optical communication over weakly ( $\alpha = 3.0, \beta = 2.7$ ) and strongly ( $\alpha = 2.3, \beta = 1.1$ ) turbulent Gamma-Gamma channels.

The BER of BPSK coherent FSO systems in large SNR regimes can be found as

$$P_{e, asym}^{BPSK} = \frac{\Gamma(\alpha - \beta) B\left(\frac{1}{2}, \beta + \frac{1}{2}\right)}{2\pi\Gamma(\alpha)} \left(\frac{\bar{\gamma}}{2\alpha\beta}\right)^{-\beta}. \quad (39)$$

From (38) and (39), we conclude that the diversity order for MPSK coherent FSO systems is equal to the smaller channel parameter, i.e.,  $\beta = \min\{\alpha, \beta\}$ , in the Gamma-Gamma turbulence.

### 3.3. Outage probability analysis

Outage probability is an important criterion for digital wireless communication networks. The outage probability for a given FSO link is defined as

$$P_{outage}(\Lambda) = \Pr(\gamma < \Lambda) = \int_0^\Lambda f_\gamma(\gamma) d\gamma \quad (40)$$

where  $\Pr(\cdot)$  denotes the probability of a event,  $\Lambda$  is a predefined outage threshold, and  $f_\gamma(\gamma)$  is the PDF of the instantaneous SNR. Thus, substituting the relationship  $\gamma = \bar{\gamma}I$  and (32) into (40), one obtains the outage probability for coherent FSO systems as

$$P_{outage}(\Lambda) = B(\alpha - \beta, 1 - \alpha + \beta) \sum_{p=0}^{\infty} \left[ \frac{a_p(\alpha, \beta)}{(p + \beta)\bar{\gamma}^{p+\beta}} \Lambda^{p+\beta} - \frac{a_p(\beta, \alpha)}{(p + \alpha)\bar{\gamma}^{p+\alpha}} \Lambda^{p+\alpha} \right]. \quad (41)$$

#### 4. System performance analysis of multichannel coherent free-space optical links

In this section, we present unified error rate studies for MRC and EGC for coherent FSO systems using an MGF approach. In a multichannel coherent FSO link, the average error rate can be expressed as [52]

$$P_e = \frac{1}{\pi} \int_0^{\frac{\pi}{2}} M_{\gamma_{mc}} \left( -\frac{\bar{\gamma}}{2 \sin^2 \theta} \right) d\theta \quad (42)$$

where  $M_{\gamma_{mc}}(\cdot)$  denotes the MGF of the multichannel combiner output instantaneous SNR. We will use (42) in the error performance study of multichannel coherent FSO systems. Here we will only mention the BER expressions for the most commonly used BPSK modulation.

##### 4.1. Analysis with maximum ratio combining

The instantaneous SNR at the output of the MRC combiner can be found as

$$\gamma_{mc,M} = \frac{RA \left( \sum_{l=1}^L I_l \right)}{q\Delta f} = \bar{\gamma} \left( \sum_{l=1}^L I_l \right) \quad (43)$$

where  $I_l$  denotes the optical signal irradiance at the  $l$ th branch. Substituting (32) into (27), we can write the MGF of  $I_l$  as power series by [41]

$$M_{I_l}(s) = \left( \sum_{p=0}^{\infty} a_p(\alpha, \beta) \Gamma(p + \beta) (-s)^{-(p+\beta)} + \sum_{p=0}^{\infty} a_p(\beta, \alpha) \Gamma(p + \alpha) (-s)^{-(p+\alpha)} \right). \quad (44)$$

With the help of a binomial expansion, the MGF of the summed RV  $\sum_{l=1}^L I_l$ , i.e.,  $M_{\sum_{l=1}^L I_l}(s) = [M_{I_l}(s)]^L$ , in terms of power series can be expressed as

$$M_{\sum_{l=1}^L I_l}(s) = \sum_{q=0}^L \binom{L}{q} \sum_{p=0}^{\infty} [\Gamma(p + \beta) a_p(\alpha, \beta)]^{(L-q)} * [\Gamma(p + \alpha) a_p(\beta, \alpha)]^{(q)} (-s)^{-p-L\beta-q(\alpha-\beta)} \quad (45)$$

where  $*$  denotes the convolution operator and  $[a_p(\alpha, \beta) \Gamma(p + \beta)]^{(n)}$  denotes  $a_p(\alpha, \beta) \Gamma(p + \beta)$  convolved  $n - 1$  times with itself. When  $n=\{0,1\}$ , we have  $[a_p(\alpha, \beta) \Gamma(p + \beta)]^{(1)} = a_p(\alpha, \beta) \Gamma(p + \beta)$  and  $[a_p(\alpha, \beta) \Gamma(p + \beta)]^{(0)} = 1$ . For such an  $L$ -branch MRC coherent FSO system, making use of (32), (42) and Laplace transforms, we can obtain the closed-form expression of the average BER as

$$P_{e,MRC} = \frac{1}{2\pi} \sum_{q=0}^L \binom{L}{q} \sum_{p=0}^{\infty} [\Gamma(p + \beta) a_p(\alpha, \beta)]^{(L-q)} * [\Gamma(p + \alpha) a_p(\beta, \alpha)]^{(q)} \times B \left( \frac{1}{2}, p + L\beta + q(\alpha - \beta) + \frac{1}{2} \right) \left( \frac{\bar{\gamma}}{2} \right)^{-p-L\beta-q(\alpha-\beta)}. \quad (46)$$

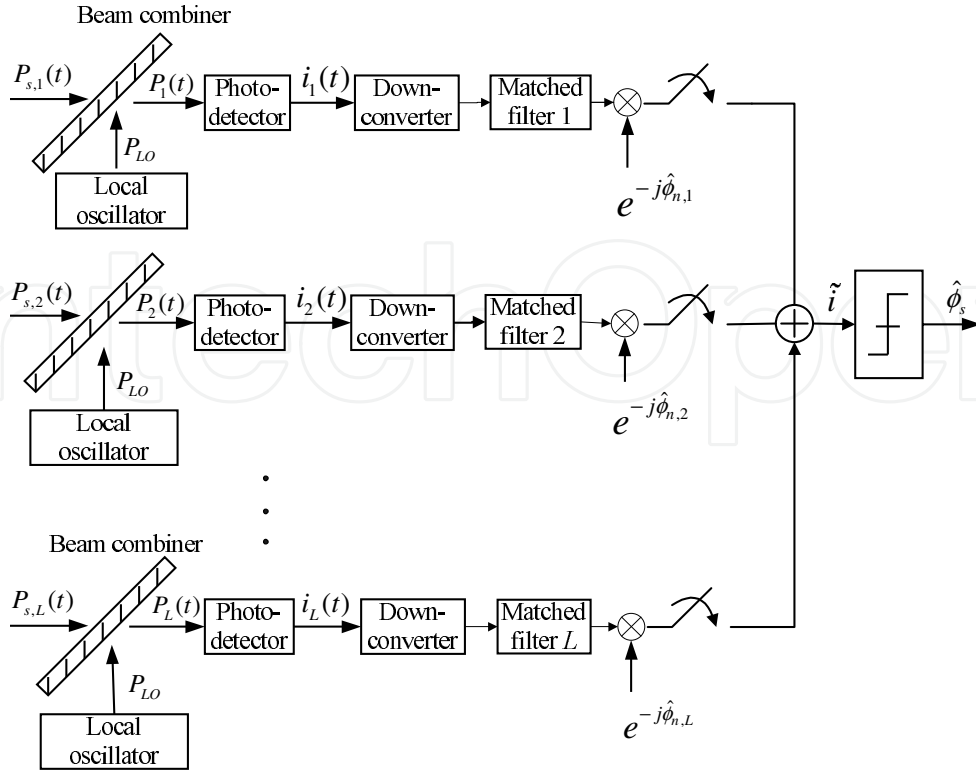


**Figure 5.** Block diagram of a coherent EGC FSO system through an atmospheric turbulence channel.

#### 4.2. Analysis with equal gain combining

For coherent FSO systems using EGC, based on the block diagram given in Fig. 5, the instantaneous SNR at the output of the combiner is found as [65]

$$\gamma_{mc,E} = \frac{RA \left( \sum_{l=1}^L \sqrt{I_l} \right)^2}{Lq\Delta f} = \frac{\bar{\gamma}}{L} \left( \sum_{l=1}^L \sqrt{I_l} \right)^2. \quad (47)$$

Based on the coherent EGC combiner SNR expression in (47), we derive the MGF of this summed RV  $X = \sum_{l=1}^L \sqrt{I_l}$ . With the PDF of  $\sqrt{I}$  and power series expansion of the modified Bessel function of the second kind, we obtain the MGF of  $\sqrt{I}$  in terms of a series expansion as

$$M_{\sqrt{I}}(s) = 2 \sum_{p=0}^{\infty} \left[ a_p(\alpha, \beta) \Gamma(2p + 2\beta) (-s)^{-2(p+\beta)} + a_p(\beta, \alpha) \Gamma(2p + 2\alpha) (-s)^{-2(p+\alpha)} \right]. \quad (48)$$

Making use of a binomial expansion, we can express the MGF of  $X$  as

$$M_X(s) = 2^L \sum_{q=0}^L \binom{L}{q} \left( \sum_{p=0}^{\infty} a_p(\alpha, \beta) \Gamma(2p + 2\beta) (-s)^{-2(p+\beta)} \right)^{L-q} \times \left( \sum_{p=0}^{\infty} a_p(\beta, \alpha) \Gamma(2p + 2\alpha) (-s)^{-2(p+\alpha)} \right)^q. \quad (49)$$

By taking the inverse Laplace transform of (49), we derive the PDF of  $X$  as

$$f_X(x) = 2^L \sum_{q=0}^L \binom{L}{q} \sum_{p=0}^{\infty} \frac{b_p^{(L-q)}(\alpha, \beta) * b_p^{(q)}(\beta, \alpha)}{\Gamma[2p + 2(L-q)\beta + 2q\alpha]} x^{2p+2(L-q)\beta+2q\alpha} \quad (50)$$

where  $b_p(\alpha, \beta) \triangleq a_p(\alpha, \beta)\Gamma(2p + 2\beta)$ . Again, with  $Y = X^2$ , the PDF of  $Y$  is found to be

$$f_Y(y) = 2^{L-1} \sum_{q=0}^L \binom{L}{q} \sum_{p=0}^{\infty} \frac{b_p^{(L-q)}(\alpha, \beta) * b_p^{(q)}(\beta, \alpha)}{\Gamma[2(p + (L-q)\beta + q\alpha)]} y^{p+(L-q)\beta+q\alpha-1}. \quad (51)$$

The MGF of  $Y$  is finally obtained as

$$M_Y(s) = 2^{L-1} \sum_{q=0}^L \binom{L}{q} \sum_{p=0}^{\infty} \frac{b_p^{(L-q)}(\alpha, \beta) * b_p^{(q)}(\beta, \alpha) \Gamma[(p + (L-q)\beta + q\alpha)]}{\Gamma[2(p + (L-q)\beta + q\alpha)]} (-s)^{-[p+(L-q)\beta+q\alpha]}. \quad (52)$$

Substituting (52) into (42), we can obtain the BER for coherent FSO links with EGC as

$$P_{e,EGC} = \frac{2^{L-2}}{\pi} \sum_{q=0}^L \binom{L}{q} \sum_{p=0}^{\infty} \frac{b_p^{(L-q)}(\alpha, \beta) * b_p^{(q)}(\beta, \alpha) \Gamma[(p + (L-q)\beta + q\alpha)]}{\Gamma[2(p + (L-q)\beta + q\alpha)]} \\ \times B\left(\frac{1}{2}, p + (L-q)\beta + q\alpha + \frac{1}{2}\right) \left(\frac{\bar{\gamma}}{2L}\right)^{-(p+(L-q)\beta+q\alpha)}. \quad (53)$$

Figure 6 plots and compares the error rates of coherent MRC and EGC systems with  $L$  receiver branches. As shown in Fig. 6, coherent MRC systems outperform EGC systems for  $L > 1$ . As the average SNR increases, the benefits from diversity reception of coherent systems are increasingly clear. It is notable that EGC has a close error performance compared to the optimal MRC systems. Therefore, EGC can be a preferable choice in designing a coherent FSO system as it provides a comparable performance to MRC and can be implemented with reduced cost, as EGC does not require the estimation of instantaneous irradiance fluctuations.

### 4.3. Truncation error analysis with a coherent diversity receiver

Up to this point, the presented error rate results are given in terms of power series. For practical calculation, we need to eliminate the infinite terms in the obtained series solutions. In this subsection, we present detailed truncation error studies for coherent FSO systems with diversity. Due to space limitations, we will study the error rate solution truncation error only in the MRC case for illustration purposes. Truncation error studies for other cases can be readily carried out.

We define the truncation error caused by eliminating the infinite terms after the first  $J + 1$  terms in the MRC series solution in (46). The error is

$$\varepsilon_{e,MRC}(J) = \frac{1}{2\pi} \sum_{q=0}^L \binom{L}{q} \sum_{p=J+1}^{\infty} [\Gamma(p + \beta)a_p(\alpha, \beta)]^{(L-q)} * [\Gamma(p + \alpha)a_p(\beta, \alpha)]^{(q)} \\ \times B\left(\frac{1}{2}, p + L\beta + q(\alpha - \beta) + \frac{1}{2}\right) \left(\frac{\bar{\gamma}}{2}\right)^{-p-L\beta-q(\alpha-\beta)}. \quad (54)$$

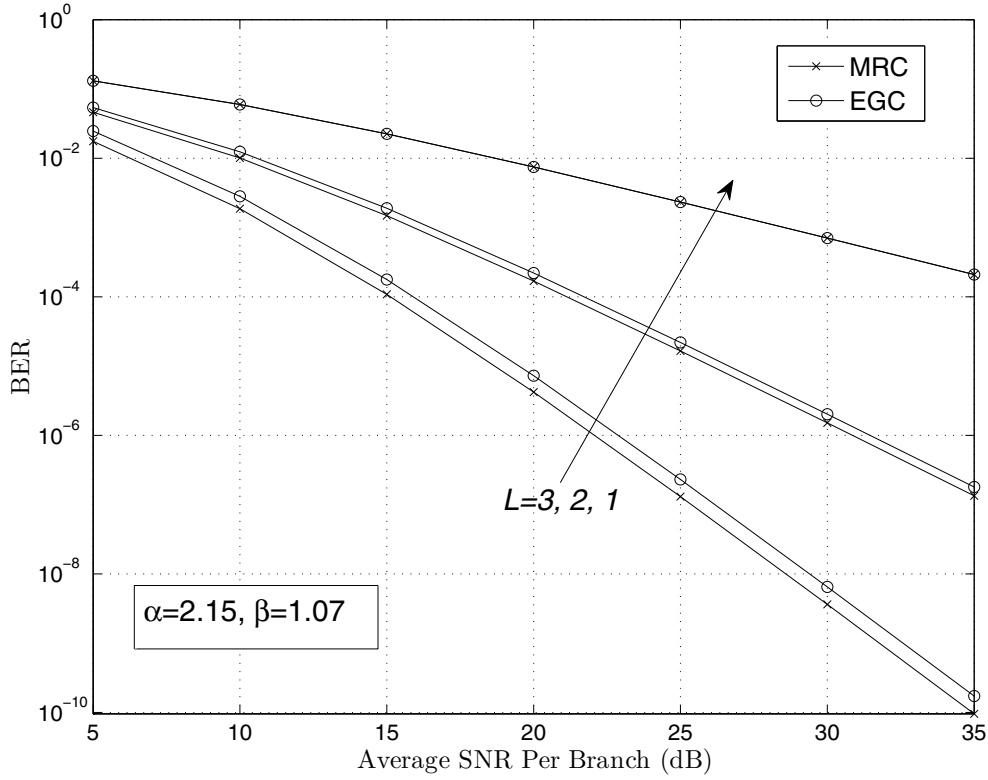


**Figure 6.** BER comparison of coherent BPSK optical communication with MRC and EGC in strongly turbulent Gamma-Gamma channels.

To facilitate the truncation error analysis, we can rewrite (54) as

$$\varepsilon_{e,MRC}(J) = \frac{1}{2\pi} \sum_{q=0}^L \binom{L}{q} \sum_{p=J+1}^{\infty} \eta_p(\alpha, \beta, L, q) \left(\frac{\bar{\gamma}}{2}\right)^{-p} \quad (55)$$

where

$$\eta_p(\alpha, \beta, L, q) = 2^{2[p+L\beta+q(\alpha-\beta)]} \frac{\Gamma^2(p+L\beta+q(\alpha-\beta)+\frac{1}{2})}{\Gamma(2p+2L\beta+2q(\alpha-\beta)+1)} [\Gamma(p+\beta)a_p(\alpha, \beta)]^{(L-q)} \quad (56)$$

$$* [\Gamma(p+\alpha)a_p(\beta, \alpha)]^{(q)} \left(\frac{\bar{\gamma}}{2}\right)^{-L\beta-q(\alpha-\beta)}.$$

Making use of a Taylor series expansion by multiplying  $x^{J+1}$  to both sides as

$$x^{J+1} \frac{1}{1-x} = x^{J+1} (1 + x + x^2 + \dots + x^n + \dots), \quad |x| < 1 \quad (57)$$

one can obtain an upper bound for the truncation error in (55) as

$$\varepsilon_{e,MRC}(J) \leq \frac{1}{\pi(\bar{\gamma}-2)} \left(\frac{\bar{\gamma}}{2}\right)^{-J} \sum_{q=0}^L \frac{\max\{\eta_p(\alpha, \beta, L, q)\} L!}{(L-q)! q!} \quad (58)$$

where we have used the identity

$$\binom{L}{q} = \frac{L!}{(L-q)!q!}. \quad (59)$$

Let us consider the first term in the infinite summation in (55). We note that the term  $\eta_p(\alpha, \beta, L, q)$  in (56) approaches zero when  $p$  (and/or  $\bar{\gamma}$ ) approaches infinity. This implies that the value of  $\eta_p(\alpha, \beta, L, q)$  decreases as the value of  $J$  increases. Therefore, it is apparent that  $\eta_p(\alpha, \beta, L, q)$  is bounded as the value of  $p$  increases. This validates our upper bound for the truncation error.

More importantly, we observe that the truncation error upper bound decreases approximately on the order of  $\bar{\gamma}^{-(J+1)}$ . This suggests an increasing accuracy of the error rate solution along with an increasing of average SNR, which is desired in a practical FSO link performance estimation.

## 5. Coherent free-space optical systems with phase noise impacts

It should be mentioned that phase noise, which can impair the error rate performance of coherent FSO systems, is assumed to be fully compensated in our previous studies in Section 3 and Section 4. The effects of spatial phase noise and atmospheric turbulence on coherent FSO systems performance have been considered together for the first time in [49]. Belmonte and Kahn studied the performance of coherent FSO links using modal phase compensation in log-normal turbulence channels [49]-[51]. In [64], the spectrum and SNR efficiencies of a variety of modulation methods were compared for coherent FSO communication through the log-normal turbulent channels. As shown in [49] and [64], phase distortion becomes an important performance limiting factor for the coherent system besides the turbulence-induced fading.

### 5.1. A revised coherent free-space optical receiver model

Here we present a revised coherent receiver model to facilitate the analysis with phase noise impacts. We consider FSO applications where a phase-locked loop (PLL) phase noise compensation mechanism is implemented at the receiver for the Gamma-Gamma turbulence channels. The optical power incident on the  $l$ th photodetector can be rewritten as [65]

$$P_l(t) = P_{s,l} + P_{LO} + 2\sqrt{P_{s,l}P_{LO}}g(t) \cos(\omega_{IF}t + \phi_s + \phi_{n,l}), \quad l = 1, 2, \dots, L \quad (60)$$

where  $P_{s,l}$  is the instantaneous incident optical signal power on the beamsplitter at the  $l$ th branch,  $P_{LO}$  denotes the local oscillator power which is assumed to be the same for all branches,  $\phi_s$  is the encoded phase information,  $\phi_{n,l}$  denotes the phase noise for the  $l$ th branch, and  $\omega_{IF} = \omega_0 - \omega_{LO}$  is the intermediate frequency, where  $\omega_0$  and  $\omega_{LO}$  denote the carrier frequency and local oscillator frequency, respectively. In (60),  $g(t)$  represents the signal pulse, which is defined as

$$g(t) = \begin{cases} \sqrt{\frac{1}{T}}, & 0 \leq t \leq T \\ 0, & \text{elsewhere} \end{cases} \quad (61)$$

where  $T$  denotes the symbol duration. In obtaining (60), we have assumed that the received optical beam and the local oscillator beam are mixed in perfect spatial coherence over a sufficiently small photodetector area. Thus, the effect of spatial phase variation is negligible, while the temporal phase variation is considered in the ensuing analysis. The incident optical power results in the photocurrent

$$i_l(t) = RP_l(t) = i_{dc,l} + i_{ac,l}(t) + n_l(t), \quad l = 1, 2, \dots, L \quad (62)$$

where we have

$$i_{dc,l} = R(P_{s,l} + P_{LO}), \quad l = 1, 2, \dots, L \quad (63)$$

and

$$i_{ac,l}(t) = 2R\sqrt{P_{s,l}P_{LO}}g(t) \cos(\omega_{IF}t + \phi_s + \phi_{n,l}), \quad l = 1, 2, \dots, L \quad (64)$$

representing, respectively, the DC and AC terms at the receiver, and  $n_l(t)$  is an AWGN process with equal variance  $\sigma^2$  for all branches. In practice, an FSO system is operated in the regime  $P_{LO} \gg P_{s,l}$ , and the DC term in (62) can be approximated by the dominant term  $RP_{LO}$ . The variance of the shot noise process  $n_l(t)$  can then be expressed by [59]

$$\sigma^2 = 2qRP_{LO}\Delta f. \quad (65)$$

Note that the DC term can be removed easily using an appropriate bandpass filter.

## 5.2. Impacts of imperfect phase noise compensation

In this section, we study the impact of phase estimation error on system performance for a coherent FSO link. We first derive the demodulator output decision statistics in the presence of phase noise compensation error. If we let  $\xi_l \triangleq 2R\sqrt{P_{s,l}P_{LO}}$ , we can express the AC current as

$$i_{ac,l}(t) = \xi_l g(t) [\cos \phi_s \cos(\omega_{IF}t + \phi_{n,l}) - \sin \phi_s \sin(\omega_{IF}t + \phi_{n,l})]. \quad (66)$$

Two real filters are then used to implement the complex filtering in the down-conversion process. The real and imaginary parts of the baseband signal are, respectively, obtained as

$$y_{c,l}(t) = \sqrt{2} \{ \xi_l g(t) [\cos \phi_s \cos(\omega_{IF}t + \phi_{n,l}) - \sin \phi_s \sin(\omega_{IF}t + \phi_{n,l})] \} \cos(\omega_{IF}t) \quad (67)$$

and

$$y_{s,l}(t) = -\sqrt{2} \{ \xi_l g(t) [\cos \phi_s \cos(\omega_{IF}t + \phi_{n,l}) - \sin \phi_s \sin(\omega_{IF}t + \phi_{n,l})] \} \sin(\omega_{IF}t). \quad (68)$$

After passing through a lowpass filter, we obtain the equivalent baseband signal  $\tilde{i}_{ac,l}(t)$ . With the relationship  $P_{s,l} = AI_l$  where  $I_l$  denotes the  $l$ th optical signal irradiance incident on the beamsplitter, the equivalent baseband signal of  $i_l(t)$  can be found as

$$\tilde{i}_l(t) = \tilde{i}_{ac,l}(t) + \tilde{n}_l(t) = \sqrt{2}R\sqrt{AP_{LO}}g(t)\sqrt{I_l}e^{j\phi_s}e^{j\phi_{n,l}} + \tilde{n}_l(t), \quad l = 1, 2, \dots, L \quad (69)$$

where  $\tilde{n}_l(t)$  is the complex-envelope of the real white Gaussian noise process with power spectral density (PSD)  $4qRP_{LO}u(\omega + \omega_{IF})$  with  $u(\cdot)$  denoting the unit step function.

After correlation and sampling, assuming perfect bit synchronization, we obtain

$$\begin{aligned}\tilde{i}_l &= \int_0^T \sqrt{2AR} \sqrt{I_l P_{LO}} g(t) e^{j\phi_{n,l}} e^{j\phi_s} g(t) dt + \int_0^T \tilde{n}_l(t) g(t) dt \\ &= \sqrt{2AR} \sqrt{I_l P_{LO}} e^{j\phi_{n,l}} e^{j\phi_s} + \tilde{n}_l, \quad l = 1, 2, \dots, L\end{aligned}\quad (70)$$

where  $\tilde{n}_l$  is a zero mean complex Gaussian RV, and its real and imaginary parts are Gaussian RVs with equal variance  $\sigma^2$ . The receiver removes the random phase noise in the optical links on all diversity branches by multiplying the received signals with the complex conjugate of the phase noise estimates from the respective channels. The output of the combiner can then be found as

$$\begin{aligned}\tilde{i} &= \sum_{l=1}^L e^{-j\hat{\phi}_{n,l}} \sqrt{2R} \sqrt{P_{s,l} P_{LO}} e^{j\phi_{n,l}} e^{j\phi_s} + \sum_{l=1}^L e^{-j\hat{\phi}_{n,l}} \tilde{n}_l \\ &= \sum_{l=1}^L e^{j\Delta\phi_l} \sqrt{2R} \sqrt{I_l A P_{LO}} e^{j\phi_s} + \nu\end{aligned}\quad (71)$$

where  $\hat{\phi}_{n,l}$  is the estimation of  $\phi_{n,l}$  at the  $l$ th branch,  $\Delta\phi_l = \phi_{n,l} - \hat{\phi}_{n,l}$  denotes the phase noise compensation error,  $\nu = \sum_{l=1}^L e^{-j\hat{\phi}_{n,l}} \tilde{n}_l$  is the complex noise term at the output of the combiner. The real and imaginary parts of the noise term  $\nu$  are Gaussian RVs with equal variance  $L\sigma^2$ . We assume that the phase noise estimations are derived from an unmodulated carrier using a first-order PLL and only Gaussian noise is present in the PLL circuit. In this case, the PDF of the phase noise compensation error  $\Delta\phi$  is given by [66]

$$f_{\Delta\phi}(\Delta\phi_l) = \frac{\exp\left(\frac{\cos(\Delta\phi_l)}{\sigma_{\Delta\phi}^2}\right)}{2\pi I_0\left(\frac{1}{\sigma_{\Delta\phi}^2}\right)}, \quad |\Delta\phi| \leq \pi\quad (72)$$

where  $\sigma_{\Delta\phi}$  denotes the standard deviation of the phase noise compensation error  $\Delta\phi_l$  for  $l = 1, \dots, L$ . We note that  $\sigma_{\Delta\phi}$  is the standard deviation of  $\Delta\phi_l$  as long as the loop SNR is large [66], which is true for practical communication links. We assume that  $\Delta\phi_1, \Delta\phi_2, \dots, \Delta\phi_L$  are independent and identical distributed (i.i.d.) RVs and the irradiance  $I_l$  is independent of  $\Delta\phi_l$ . In a typical FSO link, the turbulence has little change over the duration of hundreds of consecutive information bits, and the phase noise varies slowly compared to the high data rates in FSO systems. Therefore,  $\beta_l$  can be assumed to be a constant over the duration.

Since BPSK is assumed here, one finally obtains the demodulator decision variable by taking the real part of (71) as

$$D = \sum_{l=1}^L \sqrt{2R} \sqrt{A P_{LO}} \cos \phi_s \sqrt{I_l} \cos \Delta\phi_l + \Re\{\nu\} = \cos \phi_s \sum_{l=1}^L S_l + \nu_R$$

where  $S_l = \sqrt{2R} \sqrt{A P_{LO}} \sqrt{I_l} \cos \Delta\phi_l$ , and  $\nu_R = \Re\{\nu\}$  is a real valued zero-mean Gaussian noise RV with variance  $\sigma_{\nu_R}^2 = L\sigma^2$ . Based on the decision variable at the output of the combiner, we can find the SNR for EGC reception with phase noise compensation error as

$$\tilde{\gamma}_{EGC} = \frac{2R^2 A P_{LO}}{L\sigma^2} \left( \sum_{n=1}^L \sqrt{I_l} \cos \Delta\phi_l \right)^2 = \frac{\bar{\gamma}}{L} \left( \sum_{n=1}^L \sqrt{I_l} \cos \Delta\phi_l \right)^2.\quad (73)$$

Of great importance to the on-going investigation is the fact that the SNR in (73) is related to  $\sqrt{I_l}$  and  $\cos \Delta\phi_l$ , but it is independent of the local oscillator power.

Without loss of generality, we assume  $\phi_s = 0$ . From the expression of the decision variable in (73), we now derive the average BER for EGC with phase noise compensation error through a CHF approach. We define the cumulative distribution function (CDF) of the decision variable as

$$F_D(\xi|\phi_s = 0) = \Pr\{D < \xi|\phi_s = 0\}. \quad (74)$$

The average BER can, thus, be written as  $P_e = F_D(0|\phi_s = 0)$  when (74) is evaluated at  $\xi = 0$ .

To find  $F_D(\cdot|\phi_s = 0)$ , we write the conditional CHF of  $D$  as

$$\Phi_D(\omega|\phi_s = 0) = \Phi_{v_R}(\omega) \prod_{l=1}^L \Phi_{S_l}(\omega) = \Phi_{v_R}(\omega) [\Phi_{S_1}(\omega)]^L \quad (75)$$

for i.i.d. RVs  $S_l$ 's ( $l = 1, \dots, L$ ), where  $\Phi_{S_l}(\omega)$  is the CHF of  $S_l$  for  $l = 1, 2, \dots, L$ , and  $\Phi_{v_R}(\omega) = \exp(-L\sigma^2\omega^2/2)$  is the CHF of the Gaussian RV  $v_R$ . The CHF of  $S_1$  conditioned on  $\Delta\phi_1$  can be found to be

$$\Phi_{S_1|\Delta\phi_1}(\omega) = \Phi_z\left(\omega\sqrt{2AP_{LO}R}\cos\Delta\phi_1\right). \quad (76)$$

Averaging (76) over  $\Delta\phi_1$  gives the CHF of  $S_1$  as  $\Phi_{S_1}(\omega) = E_{\Delta\phi_1}[\Phi_z(\omega\sqrt{2AP_{LO}R}\cos\Delta\phi_1)]$ . Then, the CHF of  $D$  can be found as

$$\begin{aligned} \Phi_D(\omega|\phi_s = 0) &= [\Phi_{S_1}(\omega)]^L \Phi_{v_R}(\omega) \\ &= (E_{\Delta\phi_1}[\Phi_z(\omega\sqrt{2AP_{LO}R}\cos\Delta\phi_1)])^L \Phi_{v_R}(\omega). \end{aligned} \quad (77)$$

The CDF  $F_D(\xi|\phi_s = 0)$  can be calculated through the Gil-Pelaez formula

$$F_D(\xi|\phi_s = 0) = \frac{1}{2} - \frac{1}{\pi} \int_0^\infty \frac{\Im\{\Phi_D(\omega|\phi_s = 0)e^{-j\omega\xi}\}}{\omega} d\omega. \quad (78)$$

Finally, we find the BER with phase noise compensation errors to be

$$P_e = \frac{1}{2} - \frac{1}{\pi} \int_0^\infty \frac{\Im\{\Phi_D(\omega|\phi_s = 0)\}}{\omega} d\omega. \quad (79)$$

Substituting (77) into (79) gives the BER expression for EGC reception with phase noise compensation error. Two integrations are required to evaluate the BER performance of an  $L$ -branch EGC system using (77)-(79). In Fig. 7 and Fig. 8, the impact of phase noise is presented for  $L = 2$  and  $L = 3$  EGC FSO systems, respectively. As shown, the system will not suffer a considerable performance loss when a relatively small phase noise compensation error appears in an FSO link.

### 5.3. Differential phase-shift keying for coherent free-space optical systems

Since phase noise levels from laser sources and from atmospheric turbulence channel are time variant, the phase tracking device may be subject to carrier phase estimation error. This can lead to system performance losses and may reduce the diversity order. In this section, we present an efficient technique using DPSK for coherent FSO communications over

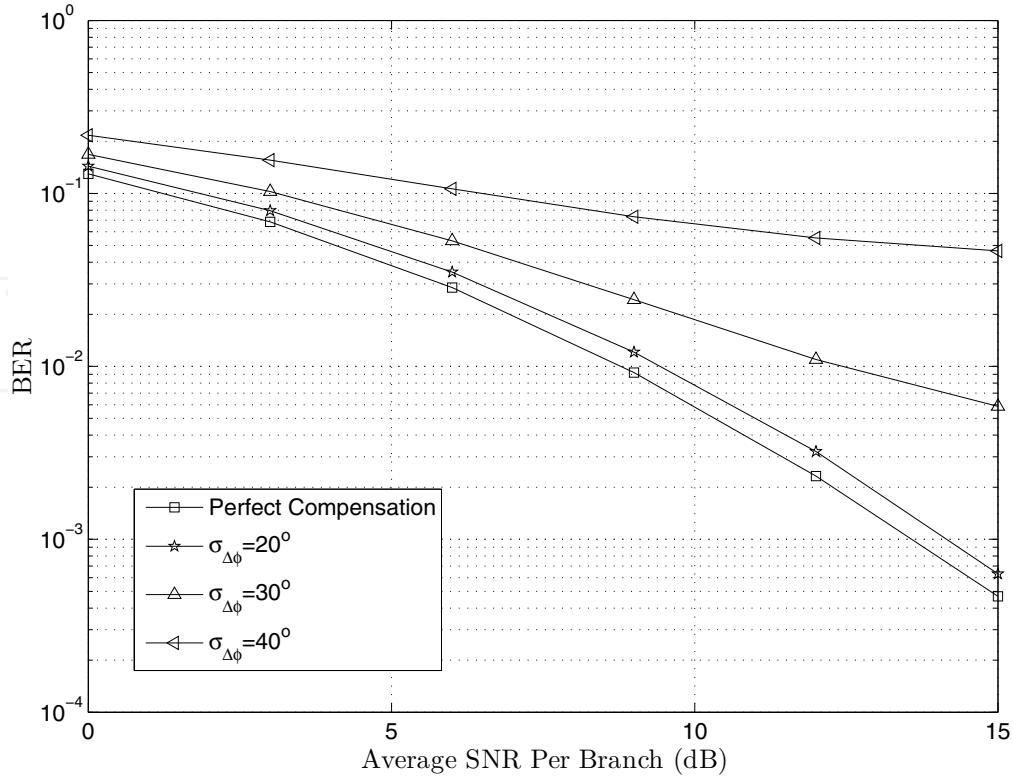


**Figure 7.** Error performance of a two-branch EGC coherent FSO system through an atmospheric turbulence channel with imperfect phase noise compensation.

atmospheric turbulence channels, which does not require estimation of the phase noise. DPSK modulation is used instead of coherent PSK for diversity reception since there is no need to estimate the phase noise.

Here, we consider a coherent FSO system employing postdetection EGC to mitigate amplitude fading as it is more suitable for differential coherent detection. Its receiver block diagram is shown in Fig. 9. The proposed FSO system is set up with  $L$ -branch wireless optical links through Gamma-Gamma turbulence. From (69) the received complex envelope at the  $l$ th branch in the  $k$ th bit interval can be written as

$$\tilde{i}_{k,l}(t) = \tilde{i}_{ac,k,l}(t) + \tilde{n}_{k,l}(t) = \sqrt{2R}\sqrt{AP_{LOG}(t)}\sqrt{I_l}e^{j\phi_{s,k}}e^{j\phi_{n,l}} + \tilde{n}_{k,l}(t) \quad (80)$$

where  $\phi_{s,k} = \phi_{s,k-1} + \Delta\phi_{s,k}$  is the differentially coded phase. Here,  $\Delta\phi_{s,k} \in \{0, \pi\}$  denotes the differential carrier phase, and the encoded phase differences are assumed to be equally likely transmitted. Due to the high data rate (on the order of Gbit/s), one can assume a "frozen atmosphere" model [45], where the characteristics of atmospheric turbulence remain constant over at least two successive symbol intervals. At the same branch, the signal in the  $(k-1)$ th bit interval can, therefore, be obtained as

$$\tilde{i}_{k-1,l}(t) = \tilde{i}_{ac,k-1,l}(t) + \tilde{n}_{k-1,l}(t) = \sqrt{2R}\sqrt{AP_{LOG}(t)}\sqrt{I_l}e^{j\phi_{s,k-1}}e^{j\phi_{n,l}} + \tilde{n}_{k-1,l}(t).$$

The shot noise processes  $\tilde{n}_{k,l}(t)$  and  $\tilde{n}_{k-1,l}(t)$  are i.i.d. complex Gaussian random processes with power spectral density  $4qRP_{LO}u(\omega + \omega_{IF})$ . In postdetection EGC reception, we can obtain the outputs of the correlator at the  $l$ th branch as

$$V_{k,l} = \int_0^T \tilde{i}_{k,l}(t)g(t)dt = \sqrt{2R}\sqrt{AP_{LOG}(t)}\sqrt{I_l}e^{j\phi_{s,k}}e^{j\phi_{n,l}} + \mu_{k,l} \quad (81)$$

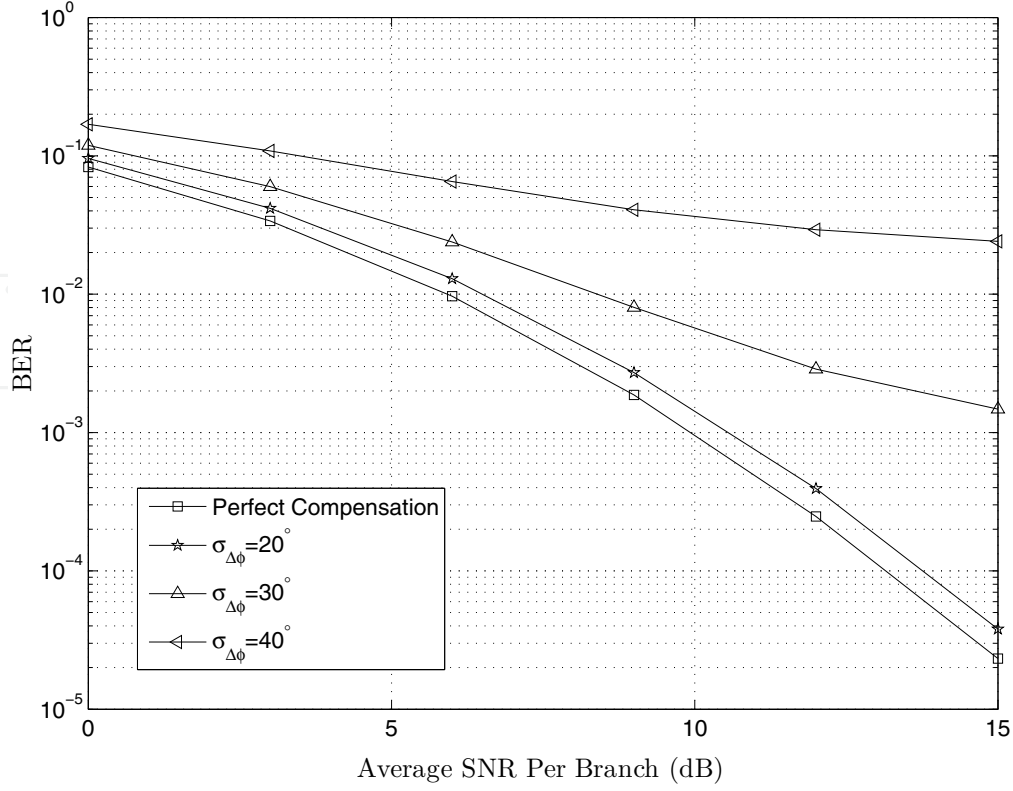


**Figure 8.** Error performance of a three-branch EGC coherent FSO system through an atmospheric turbulence channel with imperfect phase noise compensation.

and

$$V_{k-1,l} = \int_0^T \tilde{i}_{k-1,l}(t)g(t)dt = \sqrt{2}R\sqrt{AP_{LO}}\sqrt{I_l}e^{j\phi_{s,k-1}}e^{j\phi_{n,l}} + \mu_{k-1,l} \quad (82)$$

respectively. Here,  $\mu_{k,l}$  and  $\mu_{k-1,l}$  are filtered complex-valued zero mean Gaussian RVs with equal variance  $\sigma^2 = 2qRP_{LO}\Delta f$  for both the real and imaginary parts. Hence, for simplicity we drop the subscript  $l$  for the noise terms. Without loss of generality, we normalize the variance of  $\mu_k$  and  $\mu_{k-1}$  to be unity for convenience of later applications. After normalization, we obtain

$$\tilde{V}_{k,l} = \frac{R\sqrt{A}}{\sqrt{qR\Delta f}}\sqrt{I_l}e^{j\phi_{s,k}}e^{j\phi_{n,l}} + \tilde{\mu}_k = \sqrt{\tilde{\gamma}}\sqrt{I_l}e^{j\phi_{s,k}}e^{j\phi_{n,l}} + \tilde{\mu}_k \quad (83)$$

and

$$\tilde{V}_{k-1,l} = \frac{R\sqrt{A}}{\sqrt{qR\Delta f}}\sqrt{I_l}e^{j\phi_{s,k-1}}e^{j\phi_{n,l}} + \tilde{\mu}_{k-1} = \sqrt{\tilde{\gamma}}\sqrt{I_l}e^{j\phi_{s,k-1}}e^{j\phi_{n,l}} + \tilde{\mu}_{k-1} \quad (84)$$

where  $\tilde{\mu}_k$  and  $\tilde{\mu}_{k-1}$  are i.i.d. Gaussian RVs with unity variance. Therefore, the decision variable  $\tilde{D}$  at the output of the postdetection combiner is obtained as

$$\tilde{D} = \sum_{l=1}^L \tilde{U}_l = \sum_{l=1}^L \Re\{\tilde{V}_{k-1,l}^* \tilde{V}_{k,l}\} \quad (85)$$

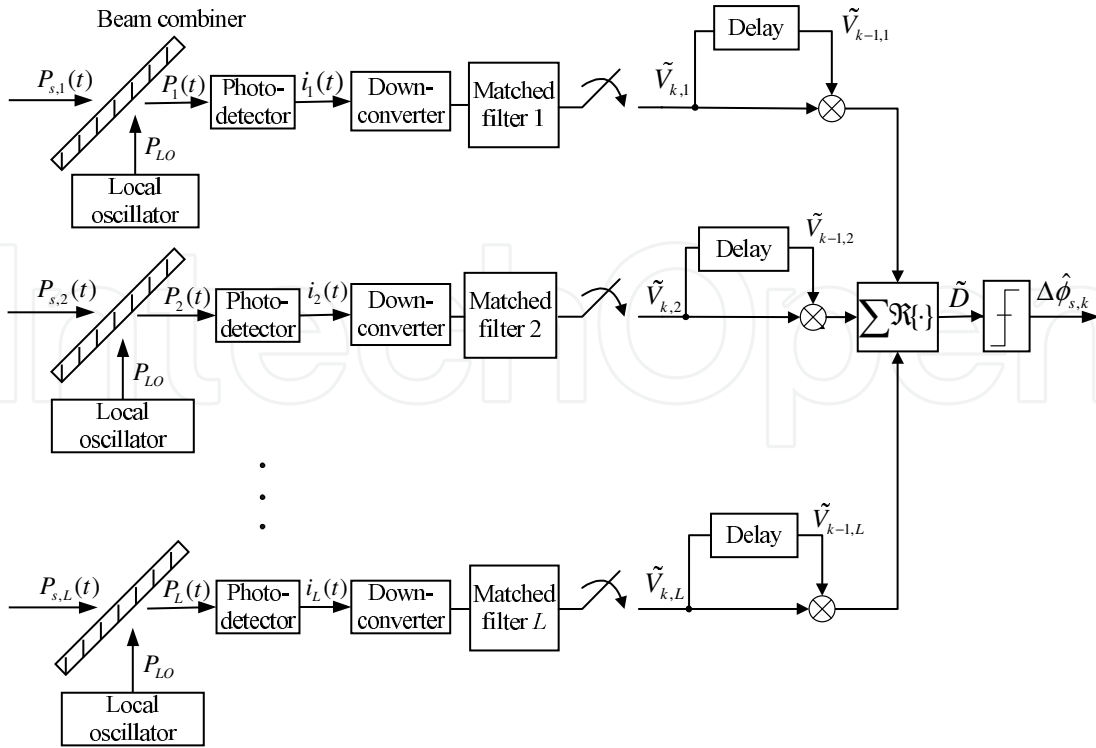


**Figure 9.** Block diagram of a coherent FSO system adopting postdetection EGC through an atmospheric turbulence channel.

where  $\tilde{U}_l = \Re\{\tilde{V}_{k-1,l}^* \tilde{V}_{k,l}\}$ . With [66, Eq. (B.5)], the CHF of  $\tilde{U}_l$  conditioned on  $I_l$  can be found as

$$\Phi_{\tilde{U}_l|\tilde{I}_l}(\omega|\Delta\phi_{s,k} = 0) = \frac{1}{\omega^2 + 1} \exp\left(-\tilde{\gamma} \frac{\omega^2 - j\omega}{\omega^2 + 1} I_l\right). \quad (86)$$

With the help of [63, Eq. 6.643(3)], averaging (86) over  $I_l$  gives the CHF of  $\tilde{U}_l$

$$\Phi_{\tilde{U}_l}(\omega|\Delta\phi_{s,k} = 0) = \frac{1}{\omega^2 + 1} M_I\left(-\tilde{\gamma} \frac{\omega^2 - j\omega}{\omega^2 + 1}\right) \quad (87)$$

where  $M_I(\cdot)$  is given by (28) or (44). For i.i.d. Gamma-Gamma turbulence, we can express the CHF of  $\tilde{D}$  as

$$\Phi_{\tilde{D}}(\omega|\Delta\phi_{s,k} = 0) = \Phi_{\tilde{U}_l}^L(\omega|\Delta\phi_{s,k} = 0) = \frac{1}{(\omega^2 + 1)^L} \left[ M_I\left(-\tilde{\gamma} \frac{\omega^2 - j\omega}{\omega^2 + 1}\right) \right]^L. \quad (88)$$

With the Gil-Pelaez formula, we can obtain the average BER for DPSK with postdetection EGC as

$$P_e = \Pr\{\tilde{D} < 0|\Delta\phi_{s,k} = 0\} = \frac{1}{2} - \frac{1}{\pi} \int_0^\infty \frac{\Im\left\{ \left[ M_I\left(-\tilde{\gamma} \cdot \frac{\omega^2 - j\omega}{\omega^2 + 1}\right) \right]^L \right\}}{\omega(\omega^2 + 1)^L} d\omega \quad (89)$$

which can be used in the BER calculation for coherent DPSK systems with (28) or (45). Figure 10 and Fig. 11 show the error performance of postdetection EGC employing DPSK in weak and strong turbulence conditions, respectively.

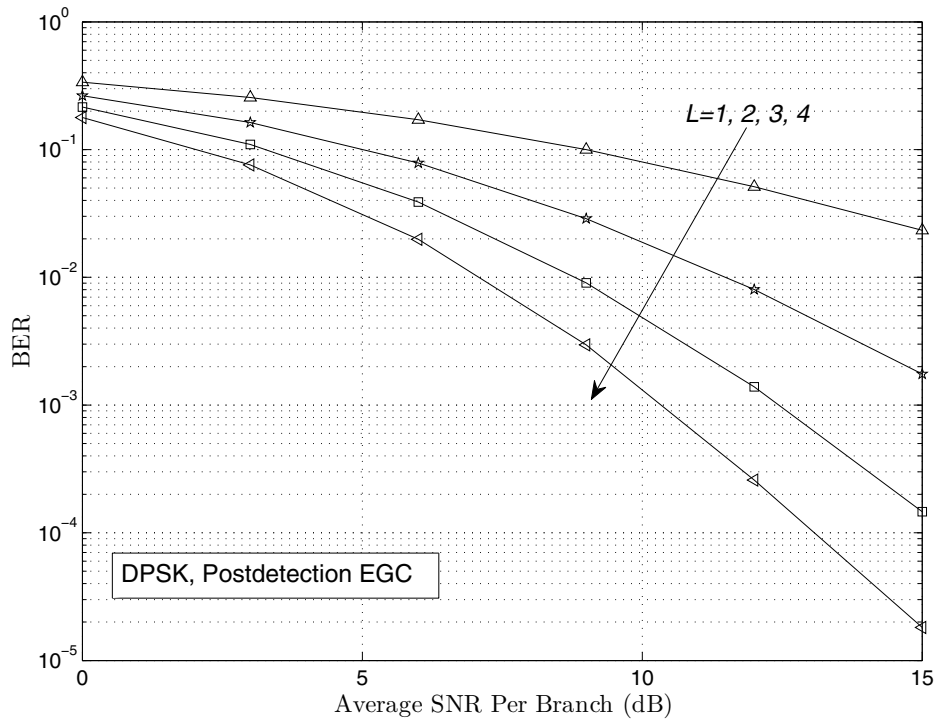


**Figure 10.** Error performance of a multi-branch postdetection EGC coherent FSO system through a strong turbulence channel with  $\alpha = 2.2$ ,  $\beta = 1.7$ .

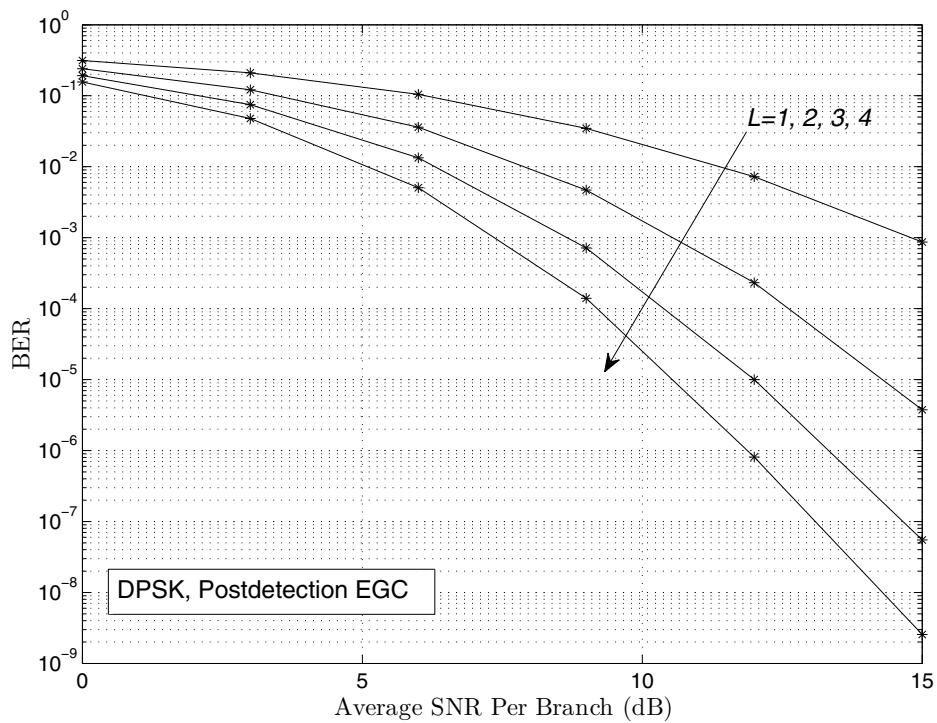


**Figure 11.** Error performance of a multi-branch postdetection EGC coherent FSO system through a weak turbulence channel with  $\alpha = 6.2$ ,  $\beta = 6.6$ .

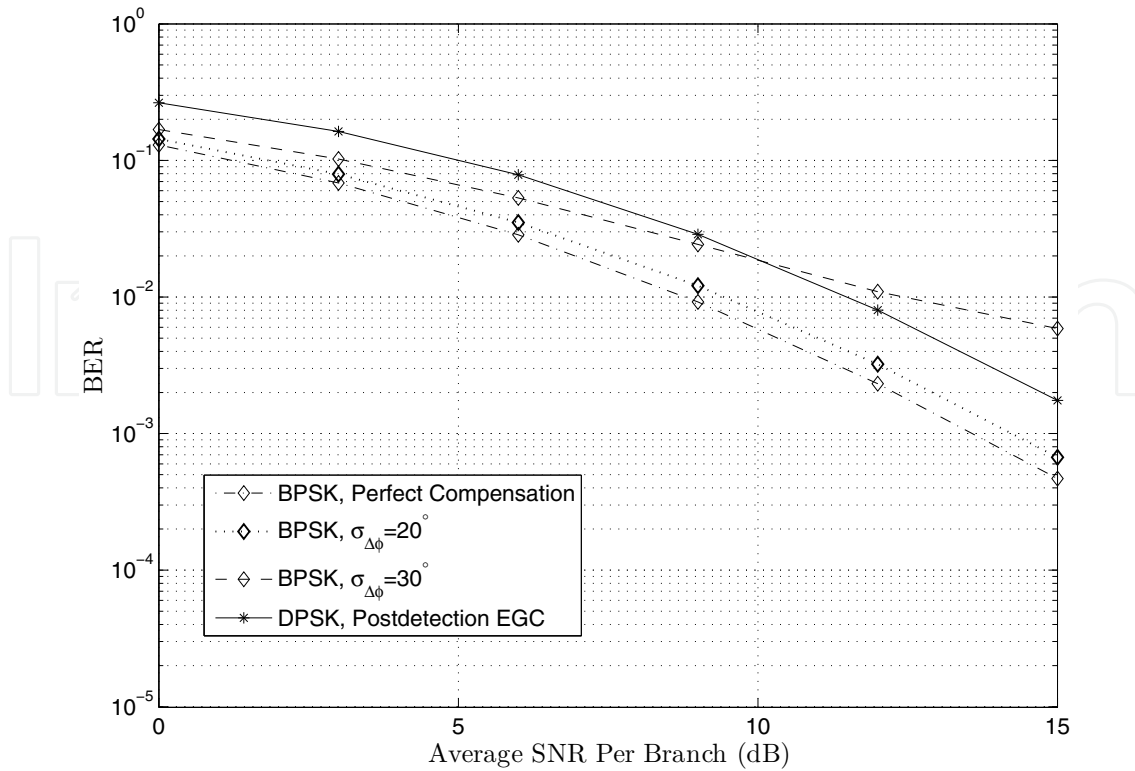


**Figure 12.** Performance comparison of two-branch EGC BPSK and postdetection DPSK FSO systems through a strong atmospheric turbulence channel with imperfect phase noise compensation.

To further illustrate the usefulness of the proposed postdetection DPSK FSO system in the presence of phase noise, we compare its error performance with that of the coherent EGC system with different standard deviations of phase noise compensation errors. As shown in Fig. 12, the proposed DPSK system is robust to the optical phase noise variations and can outperform the coherent PSK system where large phase noise compensation errors are present.

## 6. Concluding remarks and future research directions

In this chapter, we performed case studies on coherent systems for terrestrial FSO applications. We demonstrated the effectiveness of spatial diversity techniques in mitigating atmospheric turbulence effects. Important diversity reception techniques, MRC and EGC, were studied, and we showed that the EGC systems can provide comparable error performance to the optimal MRC FSO systems. We compared coherent PSK using EGC to DPSK using postdetection EGC when phase noise compensation error is present. It was found that the coherent PSK based system outperforms the DPSK based system when phase noise compensation error is small. However, it was also demonstrated that the DPSK is an excellent alternative to coherent PSK with EGC in terrestrial coherent diversity FSO communication systems where large phase noise compensation errors exist. These results can be useful in coherent FSO system design and performance evaluation. The rest of this section outlines some directions of future research on coherent FSO systems.

For practical reasons, real-time estimation of the instantaneous SNR may be difficult or expensive. Therefore, a more practical selection based combining can be proposed for

coherent FSO systems. Traditional selection combining systems must choose the branch with the largest instantaneous SNR at high operational rates. To gain the benefits of reduced complexity for selection combining, without introducing the practical challenges of maximum branch selection, signal-plus-noise (S+N) selects the largest S+N power from the multiple receiver branches. A theoretical error rate analysis as well as asymptotic analysis for S+N selection combining systems will be worthwhile to investigate to demonstrate benefits from this simplified combining scheme. Furthermore, the use of multiple optical beams to transmit information provides additional degrees of freedom to improve the optical channel liability and/or capacity. However, unlike direct detection FSO systems, the presence of phase noise will prevent multiple beams from ideal electric field mixing at the coherent receiver. To overcome this problem, the desired performance improvements can be obtained by 1. using space-time type codes; 2. implementing polarized beam transmission/reception (by applying different states of polarization to either the optical signal or carrier); 3. using wavelength multiplexing for coherent FSO systems. Specifically, for subcarrier intensity modulation and IM/DD FSO systems, Alamouti type space time coding (STC) does not offer advantages over the repetition coding. A coherent FSO system with Alamouti type STC can be of interest to study for performance comparison between different coding schemes. As an attribute of the coherent FSO technique, coherent FSO data information can also be carried through the polarization state of the electric field. Polarization multiplexing coherent FSO system can therefore be used to increase the data rate per wavelength. In addition, quantifying system performance loss due to phase noise distortion is of interest and of importance for coherent FSO links. One can study the synchronous processing with coherent PSK and differential processing with DPSK respectively for a variety of turbulence channels with a proper assumption of phase noise model (for instance, a zero mean Gaussian distribution).

## Acknowledgements

The research work presented in this chapter was supported by the University of British Columbia Internal Research Grants and the Natural Sciences and Engineering Research Council of Canada (NSERC).

## Author detail

Mingbo Niu, Julian Cheng and Jonathan F. Holzman  
*The University of British Columbia (UBC), School of Engineering, Faculty of Applied Science,  
 Kelowna, British Columbia, Canada*

## 7. References

- [1] Willebrand H, Ghuman B S (2002) *Free Space Optics: Enabling Optical Connectivity in Today's Networks*. Indianapolis, IN: Sams Publishing.
- [2] Pratt W K (1969) *Laser Communication System*. New York: Wiley.
- [3] Liu Q, Qiao C, Mitchell G, Stanton S (2005) Optical wireless communication networks for first- and last-mile broadband access, *OSA J. Opt. Netw.*, 4(12): 807-828.
- [4] Clough S A, Kneizys F X, Shettle E P, Anderson G P (1986) Atmospheric radiance and transmittance: FASCOD2, Proceedings of the Sixth Conference on Atmospheric Radiation, Williamsburg, VA, May 13th-16th. American Meteorological Society.

- [5] Anderson G P, Berk A, Acharya P K, Matthew M W, Bernstein L S, Chetwynd J H, Dothe H, Adler-Golden S M, Ratkowski A J, Felde G W, Gardner J A, Hoke M L, Richtsmeier S C, Pukall B, Mello J, Jeong L S (2000) MODTRAN4: Radiative transfer modeling for remote sensing, *Proceedings of SPIE* 4049: 176-183.
- [6] Karp S, Gagliardi R, Moran S E, Stotts L B (1988) *Optical Channels*. New York: Plenum.
- [7] Win M Z, Chen C -C, Scholtz R A (1995) Optical phase-locked loop (OPLL) for an amplitude modulated communications link using solid-state lasers, *IEEE J. Select. Areas Commun.* 13(3): 569-576.
- [8] Jafar M, O'Brien D C, Stevens C J, Edwards D J (2008) Evaluation of coverage area for a wide line-of-sight indoor optical free-space communication system employing coherent detection, *IET Commun.* 2(1): 18-26.
- [9] Kahn J M (2006) Modulation and detection techniques for optical communication systems, in *Optical Amplifiers and Their Applications/Coherent Optical Technologies and Applications*, Technical Digest (CD) (Optical Society of America), paper CThC1.
- [10] Seimetz M (2005) Multi-format transmitters for coherent optical M-PSK and M-QAM transmission, *Proceedings of 7th International Conference on Transparent Optical Networks 2*: 225-229, July 3rd-7th, Barcelona, Spain.
- [11] Andrews L C, Phillips R L, Hopen C Y, Al-Habash M A (1999) Theory of optical scintillation, *J. Opt. Soc. Am. A* 16(6): 1417-1429.
- [12] Andrews L C, Phillips R L, Hopen C Y (2001) *Laser Beam Scintillation with Applications*. Bellingham, WA: SPIE Press.
- [13] Goodman J W (1985) *Statistical Optics*, 1st ed. New York: Wiley-Interscience.
- [14] Chan V W S (2006) Free-space optical communications, *IEEE/OSA J. Lightwave Technol.* 24(12): 4750-4762.
- [15] Wireless Communications Association International. Available: <http://www.wcai.com>. Accessed 2010 March.
- [16] O'Brien D C, Katz M (2005) Optical wireless communication within fourth-generation wireless systems, *OSA J. Opt. Netw.* 4(6): 312-322.
- [17] Lee E J, Chan V W S (2004) Part 1: Optical communication over the clear turbulent atmospheric channel using diversity, *IEEE J. Select. Areas Commun.* 22(9): 1896-1906.
- [18] Lee E J, Chan V W S (2007) Diversity coherent receivers for optical communication over the clear turbulent atmosphere, *IEEE International Conference on Communications (ICC'07)*, June 24th-28th, Glasgow. pp. 2485-2492.
- [19] Lee E J, Chan V W S (2009) Diversity coherent and incoherent receivers for free-space optical communication in the presence and absence of interference, *IEEE/OSA J. Opt. Commun. Netw.* 1(5): 463-483.
- [20] Navidpour S M, Uysal M, Kavehrad M (2007) BER performance of free-space optical transmission with spatial diversity, *IEEE Trans. Wireless Commun.* 6(8): 2813-2819.
- [21] Zhu X, Kahn J M (2002) Free-space optical communication through atmospheric turbulence channels, *IEEE Trans. Commun.* 50(8): 1293-1300.
- [22] Zhu X, Kahn J M (2003) Performance bounds for coded free-space optical communications through atmospheric turbulence channels, *IEEE Trans. Commun.* 51(8): 1233-1239.
- [23] Jakeman E, Pusey P N (1978) Significance of  $K$  distributions in scattering experiments, *Phys. Rev. Lett.* 40(9): 546-550.
- [24] Parry G (1981) Measurement of atmospheric turbulence induced intensity fluctuations in a laser beam, *Optica Acta* 28(5): 715-728.
- [25] Phillips R L, Andrews L C (1981) Measured statistics of laser light scattering in atmospheric turbulence, *J. Opt. Soc. Am.* 71(12): 1440-1445.

- [26] Phillips R L, Andrews L C (1982) Universal statistical model for irradiance fluctuations in a turbulent medium, *J. Opt. Soc. Am.* 72(7): 864-870.
- [27] Al-Habash M A, Andrews L C, Phillips R L (2001) Mathematical model for the irradiance probability density function of a laser beam propagating through turbulent media, *Opt. Eng.* 40(8): 1554-1562.
- [28] Churnside J H, Clifford S F (1987) Log-normal Rician probability-density function of optical scintillations in the turbulent atmosphere, *J. Opt. Soc. Am. A* 4(10): 1923-1930.
- [29] Churnside J H, Frehlich R G (1989) Experimental evaluation of lognormally modulated Rician and IK models of optical scintillation in the atmosphere, *J. Opt. Soc. Am. A* 6(11): 1760-1766.
- [30] Uysal M, Navidpour S M, Li J (2004) Error rate performance of coded free-space optical links over strong turbulence channels, *IEEE Commun. Lett.* 8(10): 635-637.
- [31] Farid A A, Hranilovic S (2007) Outage capacity optimization for free-space optical links with pointing errors, *IEEE/OSA J. Lightwave Technol.* 25(7): 1702-1710.
- [32] Sandalidis H G, Tsiftsis T A, Karagiannidis G K, Uysal M (2008) BER performance of FSO links over strong atmospheric turbulence channels with pointing errors, *IEEE Commun. Lett.* 12(1): 44-46.
- [33] Uysal M, Li J, Yu M (2006) Error rate performance analysis of coded free-space optical links over Gamma-Gamma atmospheric turbulence channels, *IEEE Trans. Wireless Commun.* 5(6): 1229-1233.
- [34] Riediger M L B, Schober R, Lampe L (2009) Fast multiple-symbol detection for free-space optical communications, *IEEE Trans. Wireless Commun.* 57(4): 1119-1128.
- [35] Kazovsky L, Benedetto S, Willner A (1996) *Optical Fiber Communication Systems*. MA: Artech House.
- [36] Fried D L (1967) Optical heterodyne detection of an atmospherically distorted signal wave front, *Proceedings of the IEEE* 55(1): 57-68.
- [37] Wilson S G, Brandt-Pearce M, Cao Q, Baedke M (2005) Free-space optical MIMO transmission with  $Q$ -ary PPM, *IEEE Trans. Commun.* 53(8): 1402-1412.
- [38] Wilson S G, Brandt-Pearce M, Cao Q, Baedke M (2005) Optical repetition MIMO transmission with multipulse PPM, *IEEE J. Select. Areas Commun.* 9(9): 1901-1910.
- [39] Letzepis N, Holland I, Cowley W (2008) The Gaussian free space optical MIMO channel with  $Q$ -ary pulse position modulation, *IEEE Trans. Wireless Commun.* 7(5): 1744-1753.
- [40] Tsiftsis T A, Sandalidis H G, Karagiannidis G K, Uysal M (2009) Optical wireless links with spatial diversity over strong atmospheric turbulence channels, *IEEE Trans. Wireless Commun.* 8(2): 951-957.
- [41] Bayaki E, Schober R, Mallik R K (2009) Performance analysis of MIMO free-space optical systems in Gamma-Gamma fading, *IEEE Trans. Commun.* 57(11): 3415-3424.
- [42] Abou-Rjeily C, Slim A (2011) Cooperative diversity for free-space optical communications: transceiver design and performance analysis, *IEEE Trans. Commun.* 59(3): 658-663.
- [43] Ibrahim M M, Ibrahim A M (1996) Performance analysis of optical receivers with space diversity reception, *IEE Proc.-Commun.* 143(6): 369-372.
- [44] Andrews L C, Phillips R L (2005) *Laser Beam Propagation through Random Media*, 2nd ed. Bellingham, WA: SPIE Press.
- [45] Kiasaleh K. (2006) Performance of coherent DPSK free-space optical communication systems in  $K$ -distributed turbulence, *IEEE Trans. Commun.* 54(4): 604-607.
- [46] Tsiftsis T A (2008) Performance of heterodyne wireless optical communication systems over Gamma-Gamma atmospheric turbulence channels, *Electron. Lett.* 44(5): 373-375.

- [47] Sandalidis H G, Tsiftsis T A, Karagiannidis G K (2009) Optical wireless communications with heterodyne detection over turbulence channels with pointing errors, *IEEE/OSA J. Lightwave Technol.* 27(20): 4440-4445.
- [48] Li J, Liu J Q, Taylor D P (2007) Optical communication using subcarrier PSK intensity modulation through atmospheric turbulence channels, *IEEE Trans. Commun.* 55(8): 1598-1606.
- [49] Belmonte A, Kahn J M (2008) Performance of synchronous optical receivers using atmospheric compensation techniques, *Opt. Express* 16(18): 14151-14162.
- [50] Belmonte A, Kahn J M (2009) Capacity of coherent free-space optical links using atmospheric compensation techniques, *Opt. Express* 17(4): 2763-2773.
- [51] Belmonte A, Kahn J M (2009) Capacity of coherent free-space optical links using diversity combining techniques, *Opt. Express* 17(15): 12601-12611.
- [52] Niu M, Cheng J, Holzman J F, McPhail L (2009) Performance analysis of coherent free space optical communication systems with  $K$ -distributed turbulence, *IEEE International Conference on Communications (ICC'09)*, June 14th-18th, Dresden, Germany. pp. 1-5.
- [53] Niu M, Cheng J, Holzman J F (2010) Exact error rate analysis of equal gain and selection diversity for coherent free-space optical systems on strong turbulence channels, *Opt. Express* 18(13): 13915-13926.
- [54] Belmonte A, Kahn J M (2011) Field conjugation adaptive arrays in free-space coherent laser communications, *IEEE/OSA J. Opt. Commun. Netw.* 3(11): 830-838.
- [55] Aghajanzadeh S M, Uysal M (2010) Diversity-multiplexing trade-off in coherent free-space optical systems with multiple receivers, *IEEE/OSA J. Opt. Commun. Netw.* 2(12): 1087-1094.
- [56] Aghajanzadeh S M, Uysal M (2011) Multi-hop coherent free-space optical communications over atmospheric turbulence channels, *IEEE Trans. Commun.* 59(6): 1657-1663.
- [57] Lange R, Smutny B, Wandernoth B, Czichy R, Giggenbach D (2006) 142 km, 5.625 Gbps free-space optical link based on homodyne BPSK modulation, *Proceedings of SPIE* 6105: 61050A(1-9).
- [58] Kopeika N S, Bordogna J (1970) Background noise in optical communication systems, *Proceedings of the IEEE* 58(10): pp. 1571-1577.
- [59] Agrawal G P (2002) *Fiber-Optical Communication Systems*, 3rd ed. New York: Wiley.
- [60] Jakeman E, Pusey P N (1976) A model for non-Reyleigh sea echo, *IEEE Trans. Antennas Propagat.* AP-24(6): 806-814.
- [61] Niu M, Cheng J, Holzman J F (2011) Error rate analysis of  $M$ -ary coherent free-space optical communication systems with  $K$ -distributed turbulence, *IEEE Trans. Commun.* 59(3): 664-668.
- [62] Wolfram Mathworld (2011). Available: <http://functions.wolfram.com/03.04.06.0002.01>. Accessed 2011 August.
- [63] Gradshteyn I S, Ryzhik I M (2000) *Table of Integrals, Series, and Products*, 6th ed. San Diego: Academic Press.
- [64] Belmonte A, Kahn J M (2010) Efficiency of complex modulation methods in coherent free-space optical links, *Opt. Express* 18(4): 3928-3937.
- [65] Niu M, Schlenker J, Cheng J, Holzman J F, Schober R (2011) Coherent wireless optical communications with predetection and postdetection EGC over Gamma-Gamma atmospheric turbulence channels, *IEEE/OSA J. Opt. Commun. Netw.* 3(11): 860-869.
- [66] Proakis J G (2007) *Digital Communications*, 5th ed. New York: McGraw-Hill.